The Journal of Neuroscience, August 15, 2002, 22(16):7177–7194

Impairment of L-type Ca^{2+} Channel-Dependent Forms of Hippocampal Synaptic Plasticity in Mice Deficient in the Extracellular Matrix Glycoprotein Tenascin-C

Matthias R. Evers, Benedikt Salmen, Olena Bukalo, Astrid Rollenhagen, Michael R. Bösl, Fabio Morellini, Udo Bartsch, Alexander Dityatev, and Melitta Schachner

Zentrum für Molekulare Neurobiologie, Universität Hamburg, D-20246 Hamburg, Germany

The extracellular matrix glycoprotein tenascin-C (TN-C) has been suggested to play important functional roles during neural development, axonal regeneration, and synaptic plasticity. We generated a constitutively TN-C-deficient mouse mutant from embryonic stem cells with a floxed *tn-C* allele, representing a standard for future analysis of conditionally targeted mice. The gross morphology of the CNS was not detectably affected, including no evidence for perturbed nerve cell migration, abnormal oligodendrocyte distribution, or defective myelination. Despite the apparent normal histology of the hippocampus and normal performance in the water maze, theta-burst stimulation (TBS) of Schaffer collaterals elicited reduced long-term potentiation (LTP) in the CA1 region of TN-C-deficient mutants, as compared with wild-type littermates. However, high-frequency stimulation evoked normal LTP not only in CA1, but also at mossy fiber–CA3 and medial and lateral perforant path–granule cell synapses in the dentate gyrus. Low-frequency stimulation failed to induce long-term depression in the CA1 region of TN-C-deficient animals. Recordings of TBS-induced LTP in the presence of nifedipine, an antagonist of L-type voltage-dependent Ca^{2+} channels (VDCCs), did not affect LTP in TN-C-deficient mice, but reduced LTP in wild-type mice to the levels seen in mutants. Furthermore, chemical induction of a L-type VDCC-dependent LTP in the CA1 region by application of the K^+ channel blocker tetraethylammonium resulted in impaired LTP in TN-C mutants. Thus, reduction in L-type VDCC-mediated signaling appears to mediate the deficits in certain forms of synaptic plasticity in constitutively TN-C-deficient mice.

Key words: tenascin-C; knock-out mutation; extracellular matrix glycoprotein; gene targeting; hippocampus; long-term potentiation; long-term depression; CA1; CA3; dentate gyrus; water maze; TEA; L-type voltage-dependent Ca^{2+} channels; VDCC; nifedipine

Tenascin-C (TN-C) is a member of a family of closely related extracellular matrix (ECM) glycoproteins that includes TN-R, TN-X, TN-Y, and TN-W (Bristow et al., 1993; Chiquet-Ehrismann et al., 1994; Erickson, 1994; Hagios et al., 1996; Weber et al., 1998). Of the three tenascins that are detectable in the nervous system, TN-C has been studied most extensively (Faissner and Schachner, 1995; for review, see Bartsch, 1996). It is highly conserved during evolution and most prominently expressed during development of the nervous system and several non-neuronal tissues (Jones and Jones, 2000). In the nervous system, it is downregulated after maturation but persists in restricted areas that exhibit neuronal plasticity, as for instance the hippocampus (Ferhat et al., 1996).

High levels of TN-C expression at critical stages of neuronal development and regeneration and synaptic plasticity in the adult have prompted several laboratories to investigate functional properties of this ECM constituent *in vitro*. These studies have implicated TN-C in diverse functions, including cell proliferation, migration, axon guidance, and tissue development and repair. *In vitro* studies with neuronal cells have revealed that diverse functions of the molecule are localized to distinct domains and presumably also related to different cellular receptors linked to varying intracellular signal transduction pathways (Jones and Jones, 2000).

To investigate the functions of TN-C *in vivo*, two TN-C-deficient mouse mutants have been generated independently, and both have been shown to develop normally (Saga et al., 1992; Forsberg et al., 1996). However, more detailed studies on one of these mutants (Saga et al., 1992) have revealed subtle abnormalities (Fukamauchi et al., 1996; Kiernan et al., 1999; Mackie and Tucker, 1999). The interpretation of whether these abnormalities are caused by the complete lack of TN-C or a reduced expression of abnormal fragments thereof has been a matter of debate (Mitrovic and Schachner, 1995; Steindler et al., 1995; Settles et al., 1997).

Expression of TN-C is upregulated in the hippocampus after potentiation of synaptic activity *in vivo* (Nakic et al., 1996, 1998). These observations indicate a function of TN-C in synaptic plasticity, an aspect not yet investigated in TN-C-deficient mice. With the long-term aim of elucidating such a role and relating it to behavior, we have made a first step toward generating conditionally targeted mutants. To ascertain that future observations could be compared with a constitutively deficient standard, we generated a TN-C-deficient mouse starting from embryonic stem (ES) cells harboring a floxed *tn-C* allele by excision of targeted sequences *in vitro*. In this study, we report on the use of these constitutively TN-C-deficient mice to elucidate the contribution

Received Feb. 7, 2002; revised June 3, 2002; accepted June 5, 2002.

This work was supported by Deutsche Forschungsgemeinschaft Grant SCHA185/15-1 to M.S. We thank Heinz Beck (Department of Epileptology, University of Bonn, Bonn, Germany) for communicating unpublished data to us, Michael Kutsche for helpful discussions, John Neidhardt for providing the modified *neo* cassette, Emanuela Szpotowicz for technical assistance, and Eva Kronberg for animal care.

Correspondence should be addressed to Melitta Schachner, Zentrum für Molekulare Neurobiologie, Universität Hamburg, Martinistrasse 52, 20246 Hamburg, Germany. E-mail: melitta.schachner@zmnh.uni-hamburg.de.

of this ECM constituent to synaptic plasticity along the hippocampal trisynaptic circuit. We demonstrate that TN-C plays an important role in modulating L-type voltage-dependent Ca^{2+} channel (VDCC)-mediated plasticity at Schaffer collateral–CA1 synapses.

MATERIALS AND METHODS

Antibodies

The polyclonal antibodies pK7 and KAF 9–2 to TN-C and the monoclonal antibodies 619 to TN-R and 513 to myelin-associated glycoprotein (MAG) have been described (Morganti et al., 1990; Bartsch et al., 1994). Polyclonal antibodies to glutamic acid decarboxylase (GAD) were purchased from Chemicon International Inc. (Temecula, CA). A monoclonal antibody to synaptophysin was purchased from Calbiochem (Schwalbach, Germany), and monoclonal antibodies PARV-19 to parvalbumin and G-A-5 to glial fibrillary acidic protein (GFAP) were purchased from Sigma-Aldrich (Deisenhofen, Germany). For indirect immunofluorescence and Western blot analysis, Cy 3-conjugated antibodies and horseradish peroxidase-conjugated goat antibodies to rabbit or mouse IgG (all from Dianova, Hamburg, Germany) were used, respectively.

Targeting vector construction

A 129/SvJ mouse genomic library in λFix (Stratagene, Amsterdam, The Netherlands) was screened with a TN-C cDNA probe derived from parts of exons 4 and 5 (corresponding to nucleotides 2064–2395 of GenBank accession number D90343). A clone with an insert of ~18 kb covering exons 2–5 of the mouse *tn-C* gene was isolated. The replacement-type targeting vector was prepared by inserting a 1.78 kb cassette containing the phosphoglycerate kinase promotor-driven neomycin resistance cassette amplified from the pKO Scrambler V901 vector (Lexicon Genetics Inc., The Woodlands, TX) flanked by a pair of PCR-generated loxP (Hoess et al., 1982) and FRT (Andrews et al., 1985) sites into an *Eco*RV site located 117 bp upstream of exon 2, which contains the start codon (see Fig. 1*a*). A second PCR-generated loxP site adjacent to a *Bam*HI site was inserted into the *Dra*I site located 91 bp downstream of exon 2. The final targeting vector contained 1.6 kb of homologous DNA upstream (*Bgl*II–*Eco*RV fragment) of the above described cassette and 5.9 kb downstream of the single loxP site (*Dra*I–*Bam*HI fragment).

Gene targeting and generation of TN-C-deficient mouse mutants

Eighty micrograms of the *Not*I-linearized targeting vector were electroporated into 10^7 R1 ES cells (Nagy et al., 1993) using a double-pulse protocol (3 μF, 800 V prepulse; 500 μF, 240 V pulse) with the Gene Pulser system (Bio-Rad, München, Germany). G418-resistant ES cell clones harboring homologous recombination events were identified by *Bam*HI digestion of genomic DNA and Southern blot analysis using the external probe 5′A (see Fig. 1*a*). Correctly targeted ES cell clones were electroporated under the same conditions as described above with 20 μg of the Cre expression plasmid pIC-CRE (Gu et al., 1994) allowing transient expression of Cre recombinase. G418-sensitive ES cell colonies were screened for Cre-mediated excision events again by Southern blot analysis using the probe 5′A on *Bam*HI-digested DNA. Cre-recombined ES cell clones lacking the entire exon 2 were injected into C57BL/6J blastocysts. Male chimeras derived from two independently targeted ES cell clones were mated with C57BL/6J females to obtain germ line transmission. Heterozygous (*tn-C* +/−) mice were intercrossed to yield homozygous TN-C-deficient (*tn-C* −/−) and wild-type (*tn-C* +/+) littermates with a C57BL/6J-129SvJ genetic background.

Southern blot and PCR analyses

Genomic DNA (10 μg each) obtained from tail tips was digested with *Bam*HI, separated on a 0.8% agarose gel, and transferred onto Hybond-N membranes (Amersham Biosciences, Freiburg, Germany) under alkaline conditions. The PCR-generated probe 5′A (see Fig. 1*a*) was α-^{32}P-labeled using the Megaprime DNA labeling kit (Amersham Biosciences). Genotyping was performed routinely by multiplex PCR analysis using primers derived from the intron between exons 1 and 2 (5′-AGC CCC TGC CTA CCT TTT CCT AAT G-3′; see Fig. 1*a*, *1A*), from the single loxP–*Bam*HI site (5′-CCA GCT TTA TCG GAT CCA TAA CTT CG-3′; see Fig. 1*a*, *1C*), and from exon 2 (5′-CTT CGG GAG TGA GGG CAA ACA-3′; see Fig. 1*a*, *1B*). PCR was performed in 25 μl reaction mixtures containing standard buffer plus 1.5 mM $MgCl_2$ and 0.4 μM of each primer. The cycling conditions consisted of an initial 150 sec denaturing step at 94°C, followed by 30 cycles of 30 sec at 94°C, 45 sec at 65°C, and 50 sec at 72°C. A 461 bp fragment was indicative of the wild-type allele, and a 225 bp fragment was indicative of the targeted allele.

RNA preparation, Northern blot, and reverse transcription analyses

Mice were killed by cervical dislocation ($n = 6$ for each genotype), and various organs (i.e., thymus, lung) and brain regions (i.e., hippocampus, cerebellum) were quickly dissected and frozen in liquid nitrogen. Total RNA was isolated using the RNeasy system (Qiagen, Hilden, Germany). Electrophoresis and capillary blotting onto a Hybond-N membrane (Amersham Biosciences) were performed following standard procedures (Sambrook et al., 1989). Northern blots were hybridized with $5–15 \times 10^6$ cpm of a α-^{32}P-labeled TN-C cDNA probe derived from the plasmid pJT1 (Bartsch et al., 1992). For reverse transcription analysis, 250 ng of total RNA were transcribed using Omniscript Reverse Transcriptase (Qiagen) with Oligo-$(dT)_{23}$ primers. One-tenth of each reaction was amplified with the forward primer 5′-AGA GAC TTT GCT TTT CCC GAC CTG-3′ located in exon 1 and the reverse primer 5′-CAC CGC CCA CGA TTG TAG CA-3′ located in exon 3 of the *tn-C* gene (see Fig. 1*e*). A 1036 bp fragment was indicative of the wild-type mRNA, and a 454 bp fragment was indicative of an aberrant transcript lacking exon 2, namely containing exon 1 spliced directly to exon 3.

Western blot analysis

Tissue samples (cerebra and cerebella) of 7-d-old TN-C-deficient mice and wild-type littermates ($n = 6$ for each genotype) were Dounce homogenized on ice in lysis buffer [20 mM Tris, pH 7.4, 0.15 M NaCl, 0.5% (w/v) Nonidet P-40] complemented with the Complete Protease Inhibitor Mix (Roche Diagnostics, Mannheim, Germany). The homogenates were centrifuged at $20,000 \times g$ at 4°C for 30 min to remove insoluble material, and the supernatants were collected. Protein concentrations were determined with the Micro BCA protein assay (Pierce Chemical Co., Rockford, IL). Samples were subjected to 10% SDS-PAGE under reducing conditions and transferred onto a nitrocellulose membrane (Schleicher & Schuell, Dassel, Germany) following standard protocols (Towbin et al., 1979). TN-C-immunoreactive bands were detected using the polyclonal TN-C antibody pK7 (1:10,000), horseradish peroxidase-conjugated goat antibodies to rabbit IgG (1:10,000), and a chemiluminescence system (Amersham Biosciences).

Light and electron microscopy

Two-month-old TN-C-deficient mice and wild-type littermates ($n = 7$ for each genotype) were deeply anesthetized and perfused through the left ventricle with 4% paraformaldehyde and 2% glutaraldehyde in PBS, pH 7.4. Brains and eyes with attached optic nerves were removed and postfixed in the same fixative. Light and electron microscopic analysis were performed as described (Weber et al., 1999). Briefly, parasagittal sections of cerebella and cerebra were prepared with a Vibratome (Leica, Bensheim, Germany). Sections of retinas were prepared from central regions (i.e., close to the optic disk). Cerebellar, cerebral, and retinal Vibratome sections and optic nerves were incubated in 2% osmium tetroxide for 2 hr, dehydrated in an ascending series of methanol, and embedded in Epon 812 (Sigma-Aldrich). For light microscopic analysis, 3-μm-thick sections were stained with Toluidine blue and analyzed with an Axiophot (Carl Zeiss, Göttingen, Germany). Ultrathin sections were counterstained with lead citrate and examined with an EM 10C electron microscope (Zeiss).

Indirect immunofluorescence and detection of perineuronal nets

TN-C-deficient mice, 4–6 weeks old, and age-matched wild-type littermates ($n = 10$ for each genotype) were deeply anesthetized and perfused through the left ventricle with 4% paraformaldehyde in PBS, pH 7.4. Brains were removed and postfixed in the same fixative overnight at 4°C. Indirect immunofluorescence was performed as described (Weber et al., 1999). Briefly, sections (30 μm) were blocked in PBS containing 2% BSA for 2 hr followed by incubation with antibodies against parvalbumin, GAD (both 1:100 in PBS/0.1% BSA), or synaptophysin (1:100 in PBS/0.1% BSA) overnight at 4°C. After washing, sections were incubated with Cy3-conjugated antibodies to mouse IgG or rat IgG (1:300) for 2 hr at

room temperature and, after washing, mounted with Aqua-Poly/Mount (Polysciences, Warrington, PA).

Indirect immunofluorescence for the detection of TN-C (KAF 9–2; 1:100), MAG (513; 1:100), and TN-R (619; undiluted cell culture supernatant) was performed on cryostat sections. Longitudinal sections of fresh frozen optic nerves with attached retinas and parasagittal sections of fresh frozen cerebella were processed as described (Bartsch et al., 1992, 1994). Primary antibodies were detected with Cy 3-conjugated antibodies to rabbit or mouse IgG.

Visualization of perineuronal nets with the plant lectin *Wisteria floribunda* (WFA) (Sigma-Aldrich) was performed as described (Weber et al., 1999). Briefly, fixed Vibratome sections (see above) were incubated with the lectin at a final concentration of 20 μg/ml. After washing, the lectin was detected with Cy 3-conjugated streptavidin (1:600; Dianova).

Nissl and Timm's staining

For Nissl staining, fixed Vibratome sections (see above; $n = 3$ for each genotype) were washed with water followed by 70% ethanol, incubated with a 10% thionin (Sigma-Aldrich) solution (in ethanol) for 15 min at room temperature, dehydrated in ascending series of ethanol, followed by isopropanol and xylol, and mounted with EUKITT (Merck, Darmstadt, Germany). Timm's staining was performed to visualize mossy fibers in the inner molecular layer of the hippocampus. Animals ($n = 3$ for each genotype) were deeply anesthetized and transcardially perfused with 1% sodium sulfide (Sigma-Aldrich) followed by 3% glutaraldehyde and finally with 1% sodium sulfide. Brains were postfixed in the same fixative overnight at 4°C. Parasagittal brain sections (30 μm) were cut with a Vibratome (Leica), mounted onto gelatin-coated slides, and air dried overnight. Sections were washed three times in PBS (10 min each), incubated for 60 min at 30°C in Timm's solution (2.5% citric acid, 2.4% sodium citrate, 1.7% hydroquinone, 5% silver nitrate, and 25% gum arabicum; all chemicals from Sigma-Aldrich). Finally, sections were washed with tap water for 10 min, washed twice with distilled water for 5 min each, and mounted with glycerol.

Golgi impregnation

Animals ($n = 6$ for each genotype) were deeply anesthetized and transcardially perfused with 0.9% sodium chloride followed by 10% formaldehyde. Brains were postfixed in the same fixative for 1 week at room temperature and processed following a modified Golgi–Kopsch protocol. Chromation in 3.6% potassium dichromate (Sigma-Aldrich) for 5 d was followed by impregnation in 0.75% silver nitrate (Sigma-Aldrich) for 5 d. Both chromation and impregnation were repeated twice for 4 d each. Thereafter, 100 μm sagittal sections were cut with a Vibratome (Leica). Free-floating sections were dehydrated in an ascending series of ethanol, followed by methylsalicylate, isopropanol, and xylene, and mounted with DePeX (Serva).

Water maze test

Twelve- to 15-week-old males (19 TN-C-deficient mice and 19 wild-type littermates) were maintained in groups of two to three mice (at least one mouse of each genotype per group) under standard housing conditions (20 ± 1°C, 50% humidity; food and water *ad libitum*). After being subjected to several behavioral paradigms (open field, light/dark avoidance, and elevated plus maze tests), animals were housed singly for 1 week before being tested in the water maze.

Mice were trained during the dark period in a 155 cm diameter water maze (water at 20 ± 1°C, made opaque by a nontoxic white paint; 14-cm-diameter platform placed 1 cm below the water surface, white walls 20 cm above the water surface; maximal trial duration 90 sec, 15 sec on top of the platform at the end of each trial). The maze was placed at the center of the experimental room (4 × 4 m) provided with several cues and illuminated by white bulbs (light intensity was set to be 100 lux at the surface level of the maze). During the experiment, the mice were kept in a room adjacent to the experimental room illuminated by dim red light. They were transported to the water maze in a plastic cup handled by a long stick. The opening of the cup was placed toward the wall of the maze to let the mice glide into the water. Mice were started from six symmetrical starting positions in a pseudo-randomized order. After staying on the platform for 15 sec, the mice were given the opportunity to climb on a wire-mesh grid attached to a long stick and then returned to their home cage and placed under red light. We started the training with a visible platform to train all animals to associate the platform with the escape from the pool. This was done to avoid the possibility that learning of this particular feature of the task overlapped or interfered with learning of the spatial components. For the "visible platform" protocol (days 1–2, four trials per day, intertrial interval of 2 hr), the pool was surrounded by black curtains to occlude the sight of extra maze cues. The platform was cued by a 15-cm-high dark cylinder placed onto it and located pseudo-randomly in different locations across trials. For the "spatial task" acquisition, all animals were trained over 3 d (days 3–5, six trials per day, intertrial interval of 1 hr). The platform was hidden, and the curtain was removed to reveal extra maze cues. At the end of the acquisition phase, the platform was removed, and the animals were kept swimming for 60 sec (probe trial). Time spent in different areas with a surface equal to 10% of the total maze was used to test the preference of the animals for the former platform location. The next day (day 6), the hidden platform was placed at a new position, and after five acquisition trials another 60 sec probe trial (platform removed) was performed. From day 7 on, a protocol for three consecutive fast relearning trials was started ("trial-to-criterion" task) (Chen et al., 2000). Each animal was trained, for up to nine trials per day (intertrial interval of 5–8 min), for a platform location until it reached the criterion of three consecutive trials with an average escape latency of ≤15 sec before being trained for a new location on the next day. In this way, an animal was trained for one platform location over a minimum of four trials (the escape latency of the first trial was not determined) up to an open number of trials. All mice were tested until they reached the criterion for three different platform locations. The number of trials required to reach the criterion was evaluated to analyze the performance of the two genotypes. All trials were video recorded and analyzed with the video tracking system EthoVision (Noldus, Wageningen, The Netherlands).

All the data were analyzed with nonparametric statistics. Differences between the two genotypes were tested with the Mann–Whitney *U* test. Time spent in the different areas was tested against the chance level of 10% with the Wilcoxon signed rank test. To test dependent data within a genotype, Wilcoxon matched pair and Friedman tests were used. Because there is no nonparametric procedure for multifactorial analysis, a parametric ANOVA for repeated measurements having the genotype as between factor and trials as within factor was used.

Electrophysiological recordings

TN-C-deficient mice (4–6 weeks old) and their wild-type littermates were used in all electrophysiological experiments except for CA1 long-term potentiation (LTP) recordings, for which 12- to 13-week-old mice were used in addition. Hippocampal slice preparation and recordings of CA1 LTP, CA1 long-term depression (LTD), and CA3 LTP were performed as described (Eckhardt et al., 2000). All recordings and analyses were done without knowing the genotype of mice.

LTP and LTD in the CA1 region of the hippocampus. Briefly, recordings of focal field EPSP (fEPSP) were performed in the stratum radiatum with glass pipettes filled with artificial CSF (ACSF) and having a resistance of 1–2 MΩ. Schaffer collaterals were stimulated by a bipolar electrode. Basal synaptic transmission was monitored at 0.05 Hz. The inter-theta burst stimulation (TBS) interval was 20 sec, and four TBSs were applied to induce LTP. TBS consisted of 10 bursts delivered at 5 Hz. Each burst consisted of four pulses delivered at 100 Hz. Duration of pulses was 0.2 msec, and stimulation strength was set to provide fEPSPs with an amplitude of ~50% from the subthreshold maximum. For comparison of paired-pulse facilitation at different interpulse intervals, the stimulation strength was set to 25–30% of the subthreshold maximum. A voltage-dependent Ca^{2+} channel (VDCC)-dependent form of potentiation was induced by application of 25 mM tetraethylammonium (TEA), a K^+ channel blocker (Aniksztejn and Ben Ari, 1991; Huang and Malenka, 1993), for 7 min. To block the L-type VDCC-dependent component of TBS-induced LTP, nifedipine (20 μM; Sigma-Aldrich) was bath applied in the dark.

Homosynaptic LTD was induced by two trains applied at 1 Hz for 10 min with a 10 min interval between them. Stimulation strength during baseline recordings and after induction of LTD was set to 30–40% of maximal fEPSPs. Stimulation strength was set to 60–70% when 1 Hz trains were delivered. Both TBS and the protocol to induce LTD reliably produced homosynaptic NMDA receptor-dependent LTP and LTD, respectively (Eckhardt et al., 2000).

LTP in the CA3 region of the hippocampus. To record mossy fiber responses in CA3 pyramidal cells, the stimulating electrode was placed close to the inner part of the granule cell layer, and the recording electrode was placed in the stratum lucidum. Recordings and stimulations were both performed with glass pipettes filled with ACSF and having a resistance of 2 MΩ. The LTP-inducing high-frequency stimu-

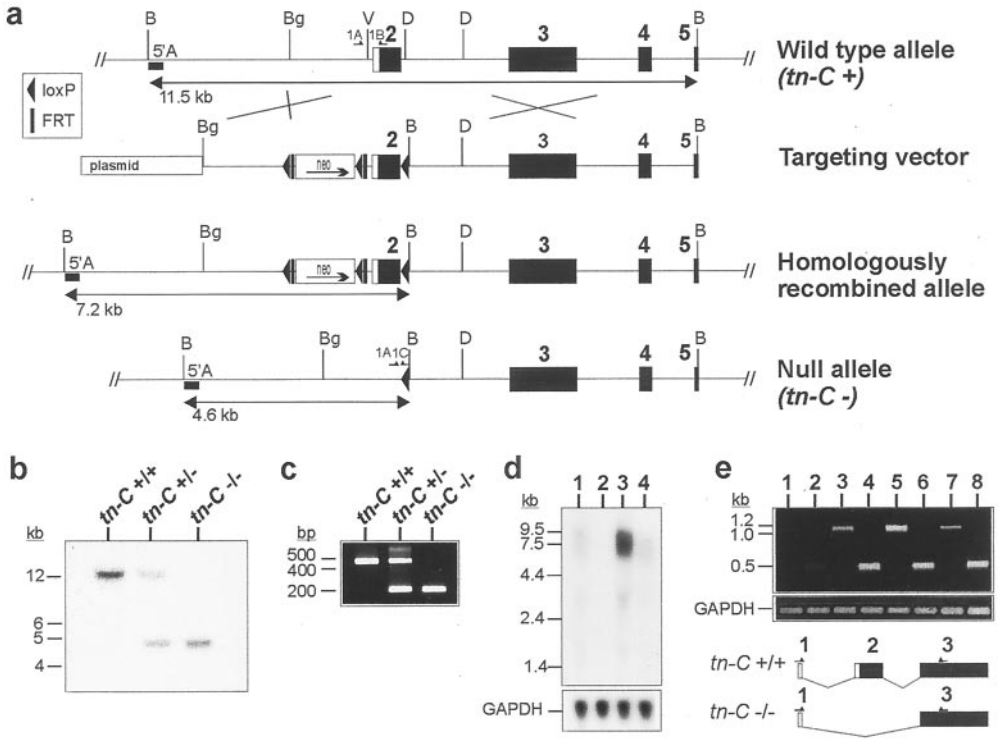

Figure 1. Targeted disruption of the murine *tn-C* gene. *a*, Diagram of a part of the murine *tn-C* gene (denoted as *tn-C* +) covering exons 2–5, the targeting vector, the targeted *tn-C* gene, and the resulting mutant (denoted as *tn-C* -) allele after Cre recombinase-mediated excision *in vitro*. Artificial introduction of a *Bam*HI site combined with the excision of the floxed exon 2 converted a 11.5 kb *Bam*HI genomic fragment indicative of the wild-type allele (*tn-C* +) to a 4.6 kb *Bam*HI genomic fragment indicative of the mutant allele (*tn-C* -). Selected restriction enzyme recognition sites are indicated as follows: *B*, *Bam*HI; *Bg*, *Bgl*II; *D*, *Dra*I; *V*, *Eco*RV. Probe *5′A* and primers *1A*, *1B*, and *1C* are indicated. *b*, Southern blot analysis of representative tail DNA samples from wild-type (*tn-C* +/+), heterozygous (*tn-C* +/−), and homozygous (*tn-C* −/−) mice. DNA was digested with *Bam*HI and subjected to hybridization using probe 5′A (*a*). *c*, Determination of genotypes by PCR. Multiplex PCR using primers *1A*, *1B*, and *1C* (*a*) as performed routinely from representative tail DNA samples. *d*, Northern blot analysis of total RNA from wild-type (*lane 1*, *3*) and TN-C-deficient mice (*lanes 2*, *4*). RNA was isolated from cerebrum (*lanes 1*, *2*) and cerebellum (*lanes 3*, *4*) of 7-d-old mice. Wild-type samples gave rise to a broad band with a size of ~6–8 kb. Note that the weak band in *lane 4* is shifted to lower molecular mass with respect to the intensive wild-type band in *lane 3*. Probing blots with a GAPDH-specific probe revealed no differences in RNA amounts loaded. *e*, RT-PCR analysis of TN-C-specific cDNAs derived from wild-type (*lanes 1*, *3*, *5*, *7*) and TN-C-deficient mice (*lanes 2*, *4*, *6*, *8*). Reverse transcription was performed on total RNA from cerebrum (*lanes 1*, *2*), cerebellum (*lanes 3*, *4*), lung (*lanes 5*, *6*), and thymus (*lanes 7*, *8*) of 7-d-old mice. In the subsequent PCR, primers were used as depicted. Note that the mutant TN-C message lacking exon 2 could be amplified from all TN-C-deficient tissues tested.

lation (HFS) consisted of trains of stimuli applied at 100 Hz for 1 sec, which were repeated four times with an interval of 20 sec. To evoke LTP exclusively in mossy fiber synapses, which are known to undergo LTP in a NMDA receptor-independent manner, the NMDA receptor antagonist AP-5 (50 μM; Tocris Cookson Ltd., Bristol, UK) was applied 15 min before and during HFS. To confirm that the fEPSPs recorded were evoked by the stimulation of mossy fibers and not by the associational–commissural pathway, an agonist of metabotropic glutamate receptors (L-CCG1, 10 μM; Tocris Cookson Ltd.) was applied at the end of each experiment. Slices in which responses were reduced by at least 70% were selected for analysis. To demonstrate dependency of the recorded LTP on protein kinase A (PKA), slices were incubated for 2 hr in a 4 ml chamber in the presence of Rp-cAMPS (100 μM; Biolog, Bremen, Germany), a membrane-permeable competitive inhibitor for PKA that was also included in the ACSF used for perfusion of slices at a concentration of 15–20 μM.

LTP in the dentate gyrus. The negative-going responses in the dentate gyrus were identified as fEPSPs evoked by stimulation of medial or lateral perforant path if they exhibited paired-pulse depression or facilitation, respectively, and changed their direction when the stimulation electrode was moved more laterally or medially. Because disinhibition is known to be an important precondition for successful induction of LTP in the dentate gyrus *in vitro* (Hanse and Gustafsson, 1992), five trains of short HFS (SHFS) were delivered in the presence of the $GABA_A$ receptor antagonist picrotoxin (100 μM; Tocris Cookson Ltd.) at 100% of supramaximal strength to elicit LTP. The intertrain interval was 20 sec, the number of pulses per train was 10, and the interpulse interval was 10 msec. Only slices showing potentiation >20% during the first 10 min after HFS were selected for further analysis.

To facilitate visual analysis of sweeps, stimulus artifacts were erased in the figures. Effects produced by stimulation or pharmacological treatments are given as mean ± SEM percentage of the baseline value. Differences between groups were tested for significance using the nonparametric Mann–Whitney *U* test and considered significant at $p < 0.05$.

RESULTS

Generation of TN-C-deficient mice

We flanked exon 2 of the murine *tn-C* gene with a loxP-FRT-pgk/neo-loxP-FRT cassette and a single loxP site by homologous recombination in R1 ES cells (Nagy et al., 1993) (Fig. 1*a*). G418-sensitive ES cell clones harboring the desired recombination event were identified by Southern blot analysis (data not shown). The *neo* selection marker and the entire exon 2 with adjacent intronic sequences were excised *in vitro* by transient expression of Cre recombinase. A sequence coding for the signal peptide and tenascin assembly (TA) domain was thus deleted, leading to a predicted frameshift in the TN-C transcript [see also Forsberg et al. (1996)]. Cre-recombined, G418-sensitive ES cell clones were identified by Southern blot analysis with the probe 5′A flanking the sequence included in the targeting vector. The

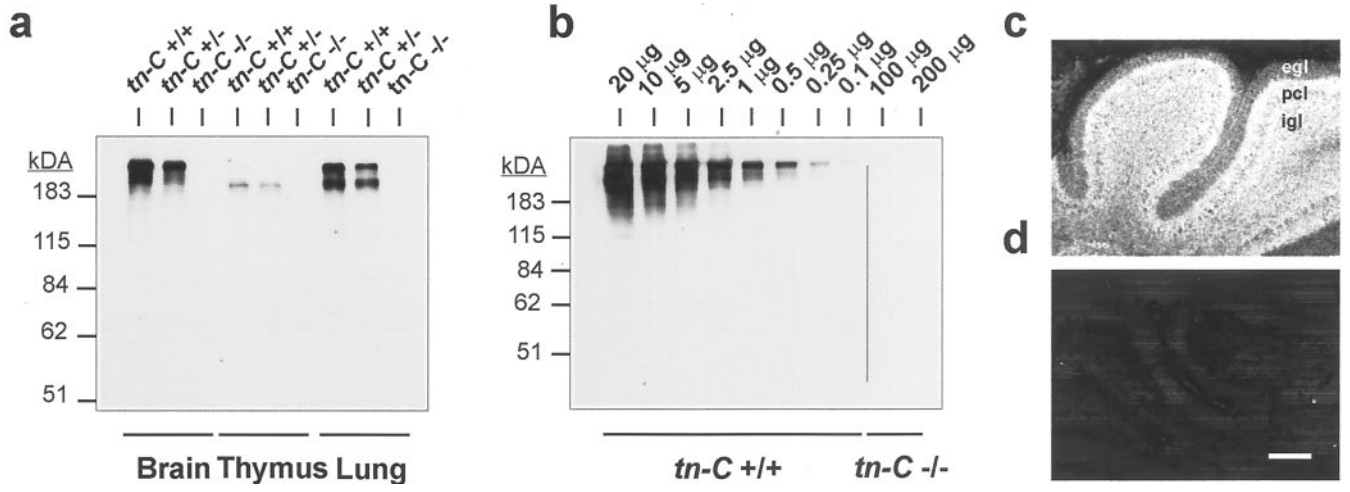

Figure 2. Western blot and immunohistological analysis of TN-C-deficient mice. *a*, Western blot analysis of crude protein extracts from brain, thymus, and lung tissue of 7-d-old mice from the indicated genotypes (*tn-C* +/+, *tn-C* +/−, and *tn-C* −/−) using polyclonal TN-C antibody pK7. In each lane, 10 μg of total protein was loaded. Intense immunoreactive bands specific for TN-C were easily detected in tissues from wild-type mice, but no signals were detectable in samples from TN-C-deficient animals. Heterozygous mice showed a reduced signal intensity of TN-C-immunoreactive bands. *b*, Quantitation of the TN-C protein content in different genotypes. The indicated amounts of total protein from cerebra of 7-d-old wild-type (*tn-C* +/+) and homozygously TN-C-deficient littermates (*tn-C* −/−) were applied and detected after blotting with the polyclonal TN-C antibody pK7. In wild-type animals, TN-C was detectable in as little as 0.1 μg total protein, whereas in mutant littermates no band was detectable even in 200 μg total protein. Molecular weight markers are indicated at the left margins in kilodaltons. *c*, *d*, Immunohistological localization of TN-C by indirect immunofluorescence on fresh frozen sections of cerebella of 7-d-old wild type mice (*c*) and TN-C-deficient littermates (*d*) using polyclonal antibody KAF 9–2. Intense TN-C immunoreactivity is visible on sections from wild-type mice, whereas no immunoreactivity is detectable in age-matched TN-C deficient littermates. Sections incubated only with secondary antibody showed no immunoreactivity (data not shown). *egl*, External granular layer; *igl*, internal granular layer; *pcl*, Purkinje cell layer. Scale bar (shown in *d*): *c*, *d*, 150 μm.

presence of the artificially introduced *Bam*HI site (Fig. 1*a*) and the lack of exon 2 were indicated by the appearance of a 4.6 kb band in addition to the wild-type signal at 11.5 kb. The expected band pattern is identical to the one obtained from DNA of heterozygous offspring (Fig. 1*b*, *lane* labeled *tn-C* +/−). Two independent ES cell clones were used to generate chimeric mice. Germ line transmission was achieved with chimeras from both ES cell clones as evident from Southern blots (Fig. 1*b*, *lane* labeled *tn-C* +/−). Homozygous TN-C-deficient (*tn-C*−/−) and wild-type littermates (*tn-C* +/+) used during this study were obtained from intercrossings of heterozygous (*tn-C* +/−) animals at Mendelian frequencies. Genomic DNA samples from wild-type, heterozygous, and homozygous mice were digested with *Bam*HI and subjected to Southern blot analysis. Analysis with the probe 5′A confirmed the pattern expected from the successful homologous recombination and the subsequent Cre recombinase-mediated excision event *in vitro* (Fig. 1*b*). Multiplex PCR was performed to determine routinely the genotype of animals (Fig. 1*c*). TN-C-deficient mice developed normally by gross inspection and had a normal life span and fertility.

To test whether the mutated *tn-C* allele is transcribed, Northern blot and RT-PCR analyses were performed. After hybridizing with a mouse cDNA probe derived from plasmid pJT1 (Bartsch et al., 1992), Northern blot analysis of total RNA from cerebella of 7-d-old TN-C-deficient mice revealed very weak expression levels of a mutated TN-C transcript (Fig. 1*d*, *lane 4*). In contrast, a strong signal for the wild-type TN-C message of a size of ~6–8 kb was easily detectable in total RNA from cerebella and to a lesser extent in total RNA from cerebra of 7-d-old wild-type littermates (Fig. 1*d*, *lanes 1*, *3*). As expected, the mutant transcript appeared to be shorter than the message expressed in wild-type tissues (Fig. 1*d*, compare *lanes 3*, *4*). Expression levels of this aberrant message were almost undetectable in total RNA from TN-C-deficient cerebra of the same developmental stage (Fig. 1*d*, *lane 2*), but RT-PCR analysis confirmed transcription in all tissues from 7-d-old TN-C-deficient mice that were tested (cerebrum, cerebellum, lung, and thymus) (Fig. 1*e*). Furthermore, by using primers derived from sequences of exon 1 and 3, this approach indicated that the mutated mRNA contained exon 1 directly spliced to exon 3 (Fig. 1*e*). The nucleotide sequence of this aberrant message was determined and revealed that the lack of exon 2 led to a frame shift, as it was described by Forsberg et al. (1996) for an independently generated TN-C-deficient mutant. By replacing the coding region of exon 2 with a neomycin cassette, these authors kept both splice sites intact but also detected mainly the same unexpected splicing event. In the other published TN-C-deficient mutant, Saga et al. (1992) replaced parts of exon 2 and the 5′ region of intron 2 with a β-galactosidase gene and a neomycin cassette. Only when these authors used a β-galactosidase gene-specific probe could transcription of the mutated *tn-C* gene be detected.

To analyze whether the mutant mRNA was translated into a truncated protein, we analyzed in detail the amount of TN-C proteins in the mutant. The TN-C protein content was evaluated in thymus, lung, and cerebellum of 7-d-old TN-C-deficient and age-matched wild-type mice by Western blot analysis (Fig. 2*a*). All of these tissues are known to express high levels of TN-C at this developmental stage (Bartsch et al., 1992). As expected, TN-C protein was easily detected with the polyclonal antibody pK7 in protein extracts of all three tissues tested from wild-type mice (Fig. 2*a*, *lanes* labeled *tn-C* +/+). A significant reduction of TN-C immunoreactivity was observed in protein extracts from heterozygous tissues (Fig. 2*a*, *lanes* labeled *tn-C* +/−). Samples from homozygous TN-C-deficient littermates did not give rise to TN-C immunoreactive signals (Fig. 2*a*, *lanes* labeled *tn-C* −/−). To study the possibility of a residual expression of TN-C or

truncated forms thereof, we performed quantitative immunoblot analysis using the polyclonal TN-C antibody pk7 (Fig. 2*b*). In crude lysates from cerebra of 7-d-old wild type mice, TN-C immunoreactivity was detectable in as little as 0.1 μg of total protein (Fig. 2*b*). In contrast, no immunoreactive bands were visible in 200 μg of total protein from TN-C-deficient tissue (Fig. 2*b*). Thus, if residual TN-C protein should be expressed in the mutant, it comprises <0.05% of the wild-type level. Immunohistological analysis of sections from fresh frozen cerebella with the polyclonal antibodies KAF 9–2 (Fig. 2*c*,*d*) and pK7 (data not shown) confirmed the result obtained by immunoblot analysis. Although intense TN-C immunoreactivity was visible on wild-type sections (Fig. 2*c*), no specific signal was detectable in mutant cerebella (Fig. 2*d*). Thus, we consider our TN-C-deficient mouse to be a true null mutant. Forsberg et al. (1996) proved TN-C deficiency in their mutant using the same antibodies for Western blot analysis. TN-C protein levels in the mutant described by Saga et al. (1992) were indicated to be below 1% of wild-type levels on the basis of experiments with variable exposure times of Western blots using monoclonal TN-C antibodies (Settles et al., 1997). However, the latter mutant has been controversial. Mitrovic and Schachner (1995) reported the detection of residual amounts of a truncated TN-C by Western blot analysis and immunocytochemistry, whereas Steindler et al. (1995) and Settles et al. (1997) could not detect any residual TN-C proteins in the same mutant using the same antibodies.

Morphological analysis

Cell culture experiments have implicated TN-C in diverse functions during neural development, including neurite elongation, nerve cell migration, or inhibition of axonal regeneration (Faissner and Schachner, 1995; for review, see Bartsch, 1996). TN-C is strongly expressed in the developing cerebellar cortex by astrocytes and Golgi epithelial cells and remains expressed at high levels in the adult (Bartsch et al., 1992). Moreover, TN-C has been demonstrated to promote neurite extension from cerebellar granule cells and migration of granule cells from the external to the internal granular layer *in vitro* (Husmann et al., 1992). However, light microscopic inspection of the cerebellar cortex of TN-C-deficient mutants revealed an apparently normal histoarchitecture (Fig. 3*b*). All cortical layers formed normally with a thickness indistinguishable from that of wild-type mice (Fig. 3, compare *a*, *b*). There was also no evidence for ectopically positioned granule cells or other neural cell types in mutant cerebella (Fig. 3*b*). Moreover, electron microscopic analysis revealed no obvious defects of Golgi epithelial cells. For instance, end feet of Golgi epithelial cells formed an ultrastructurally intact glial-limiting membrane (data not shown). Ultrastructural abnormalities of cerebellar nerve cell types, and in particular of parallel fibers, were also not detectable (data not shown).

The retina is another CNS structure displaying high levels of TN-C expression during development and significant levels of immunoreactivity in the adult (Bartsch et al., 1994). Again, obvious morphological alterations of TN-C-deficient retinas were not observed (Fig. 3*d*), and all retinal cell types of TN-C-deficient mice were positioned appropriately.

To evaluate the possibility that the lack of TN-C is compensated by increased levels of TN-R expression, we performed TN-R immunohistochemistry on brain sections from 2-month-old TN-C mutants. In the cerebellar cortex of wild-type mice, TN-R immunoreactivity was homogeneously distributed in the molecular layer and internal granule cell layer and particularly intense in the white matter. A similar distribution and intensity of TN-R positivity was observed in the cerebellar cortex of TN-C-deficient littermates (Fig. 3, compare *e*, *f*).

Examination of TN-C-deficient optic nerves

TN-C is strongly expressed in the developing optic nerve and remains expressed at high levels in the unmyelinated retinal end of the adult nerve (Bartsch et al., 1994). Substrate-bound TN-C is a nonadhesive substrate for cells of the oligodendrocyte cell lineage when offered as a patterned substrate (Bartsch et al., 1994). In addition, migratory activity of oligodendrocyte progenitor cells is reduced on homogenous TN-C substrates (Kiernan et al., 1996). We therefore hypothesized that elevated levels of TN-C at the retinal end of the optic nerve prevent migration of oligodendrocyte progenitor cells into the retina and as a consequence intraretinal formation of myelin (Bartsch et al., 1994). Thus, we analyzed in detail the primary visual pathway of TN-C-deficient mice and, in particular, the distribution of oligodendrocytes and myelin along retinal ganglion cell axons. The distribution of oligodendrocytes and myelin in 2-month-old wild-type (Fig. 3*g*) and TN-C-deficient mice (Fig. 3*i*) was visualized in longitudinally sectioned optic nerves using MAG antibodies. Strong and homogenously distributed MAG immunoreactivity was observed in distal regions of optic nerves of both genotypes. However, a sharp transition from a MAG-immunoreactive to a MAG-immunonegative region was observed at the retinal end of the optic nerve of both genotypes (Fig. 3*g*,*i*), reflecting the characteristic differential distribution of oligodendrocytes and myelin in the primary visual pathway of mice. As a next step, we studied optic nerves of 2-month-old TN-C mutants and age-matched wild-type mice at the ultrastructural level. Astrocytes are the cellular source of TN-C in developing optic nerves. Electron microscopic analysis revealed a normal ultrastructure of astrocytes and an apparently normal structure of the glial-limiting membrane of TN-C-deficient nerves (Fig. 3*k*). The ultrastructure of retinal ganglion cell axons was also not altered detectably (Fig. 3*k*,*l*) when compared with wild-type nerves (data not shown). There was also no evidence for a disturbed myelination in TN-C-deficient optic nerves. Virtually all ganglion cell axons of mutant mice were surrounded by a myelin sheath (Fig. 3*k*). Inspection of TN-C-deficient optic nerves at higher magnification revealed the presence of myelin sheaths with a normal ultrastructure (Fig. 3*l*).

Normal histoarchitecture of the TN-C-deficient hippocampus

Levels of TN-C immunoreactivity are high in the developing hippocampus and decrease during maturation (Ferhat et al., 1996). In the adult rat, residual TN-C immunoreactivity is detectable in the strata oriens and radiatum of the CA1, stratum oriens of the CA3 region, alveus, and the molecular layer of the dentate gyrus, where it is most prominent in the hilar region (Nakic et al., 1998). We obtained similar results on fresh frozen sections from 4- to 6-week-old wild-type mice by indirect immunofluorescence using the polyclonal TN-C antibody KAF 9–2. As in rats, TN-C expression was weak and diffusely distributed (Fig. 4*a*, CA1). TN-C-deficient littermates showed no detectable immunoreactivity (Fig. 4*b*).

To further investigate the functional role(s) of TN-C in the adult hippocampus, we studied the histoarchitecture of the hippocampal formation of TN-C-deficient mutants. CA1 through CA3 regions and dentate gyrus of the hippocampus appeared

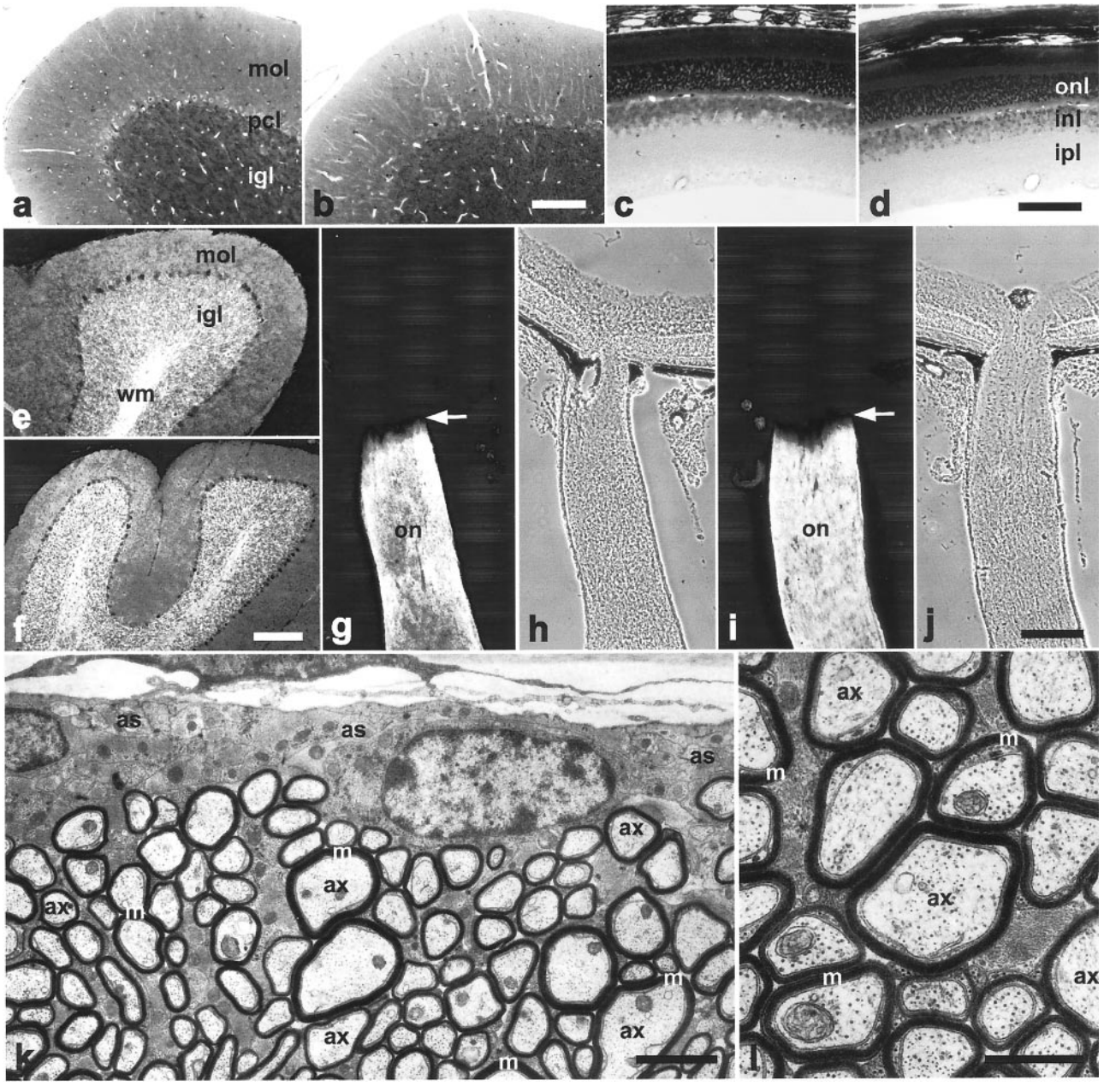

Figure 3. Morphological and immunohistochemical analysis of TN-C-deficient mice. Light microscopic analysis of the cerebellar cortex (*a*, *b*) and retina (*c*, *d*) of 2-month-old wild-type (*a*, *c*) and TN-C-deficient (*b*, *d*) mice demonstrates an apparently normal histoarchitecture of both CNS structures in the mutant. All cerebellar (compare *a*, *b*) and retinal (compare *c*, *d*) layers of TN-C-deficient animals display a normal thickness, and there is no evidence for ectopically positioned cell types in TN-C-deficient tissues. TN-R immunoreactivity in the cerebellar cortex of wild-type mice (*e*) is homogeneously distributed in the molecular layer (*mol*) and internal granule cell layer (*igl*) and is accumulated in the white matter (*wm*). A similar distribution and intensity of TN-R positivity is detectable in the cerebellar cortex of TN-C-deficient mice (*f*). The distribution of oligodendrocytes and myelin in the optic nerve (*on*) of adult wild-type (*g*) and TN-C-deficient (*i*) mice was visualized with MAG antibodies (*h* and *j* are the phase-contrast images of *g* and *i*, respectively). MAG immunoreactivity is absent from the retinal end of the optic nerve and from the retina of both genotypes. *Arrows* in *g* and *i* indicate the transition zone from myelinated to nonmyelinated segments of retinal ganglion cell axons. Electron microscopic analysis of optic nerves from TN-C-deficient mice (*k*) revealed a normal ultrastructure of the meninges and glia limitans (*k*). Virtually all ganglion cell axons of mutant mice (some labeled with *ax* in *k* and *l*) are surrounded by a myelin sheath (some labeled with *m* in *k* and *l*). Analysis at a higher magnification demonstrates the presence of ultrastructurally intact CNS myelin sheaths in TN-C-deficient optic nerves. *as*, Astrocyte; *ax*, axons; *igl*, internal granule cell layer; *inl*, inner nuclear layer; *ipl*, inner plexiform layer; m, myelin sheath, *mol*, molecular layer; *on*, optic nerve; *onl*, outer nuclear layer; *pcl*, Purkinje cell layer; *wm*, white matter. Scale bars: (shown in *b*) *a*, *b*, 100 μm; (shown in *d*) *c*, *d*, 100 μm; (shown in *f*) *e*, *f*, 200 μm; (shown in *j*) *g–j,* 200 μm; *k,* 2 μm; *l,* 1 μm.

histologically normal as judged from Nissl-stained sections (Fig. 4, compare *c*, *d*) and neurofilament immunohistochemistry (data not shown). No significant difference in the distribution of astrocytes was detectable between genotypes, as suggested from immunostainings with antibodies reactive to GFAP (data not shown). Finally, neither synaptophysin immunoreactivity nor Timm's staining revealed abnormalities in the laminated organization of the CA3 region or mossy fiber projection (Fig. 4, compare *e* and *f*, *g* and *h*). Weber et al. (1999) demonstrated abnormal perineuronal nets and Saghatelyan et al. (2001) de-

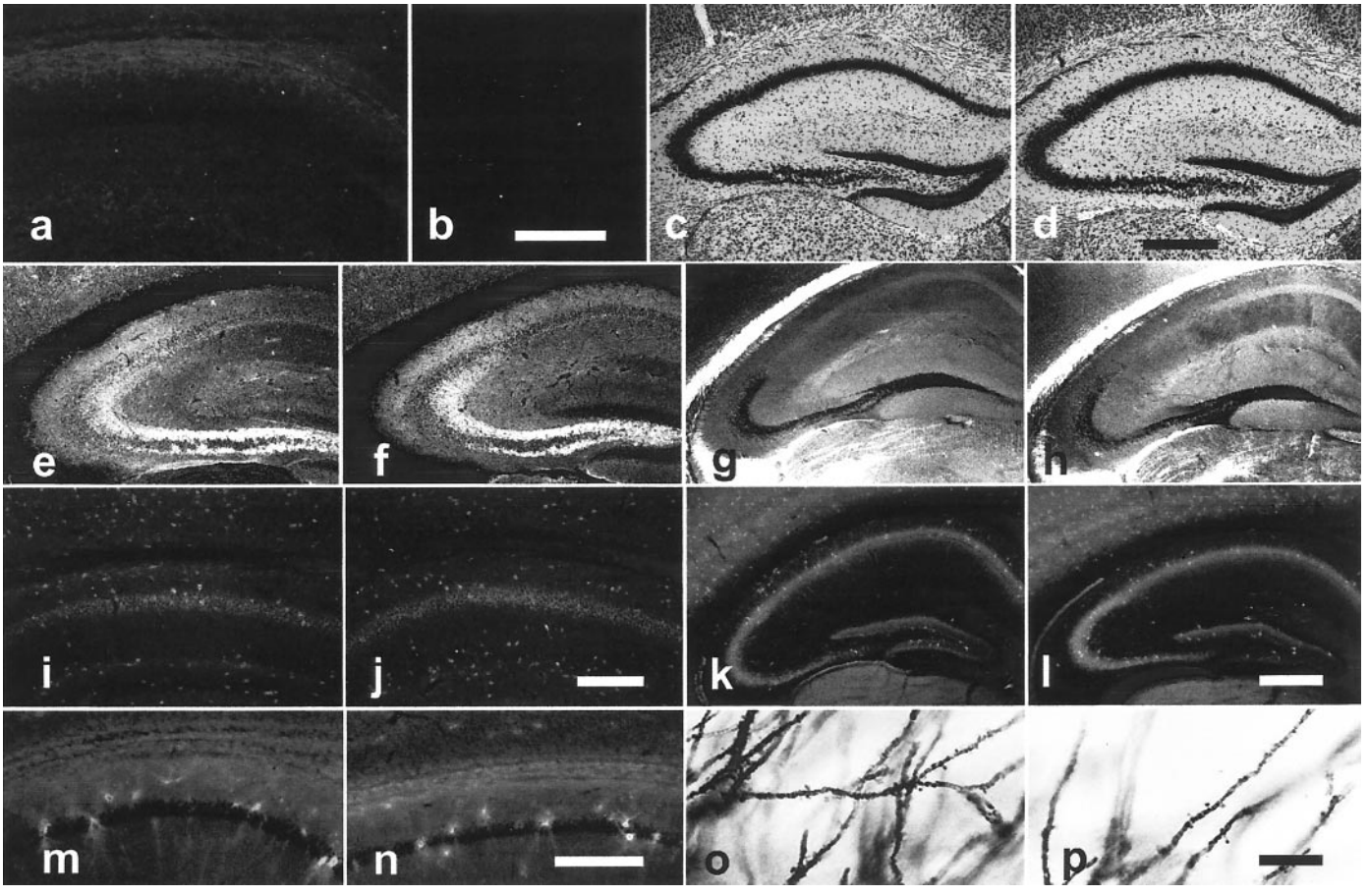

Figure 4. Hippocampal morphology of TN-C-deficient mice. *a*, *b*, TN-C immunoreactivity was detectable in the hippocampal CA1 region of 5-week-old wild-type mice (*a*) by indirect immunofluorescence using the polyclonal antibody KAF 9–2. Specificity of weak signals is demonstrated by comparison with TN-C-deficient littermates (*b*). *c*, *d*, Nissl staining revealed an apparently normal histology of CA1 through CA3 regions and of the dentate gyrus of TN-C-deficient mutants (*c*) when compared with wild-type mice (*d*). *e–h*, Immunohistochemical localization of the presynaptic marker synaptophysin (*e*, *f*) and Timm's staining (*g*, *h*) revealed a similar laminated organization of the CA3 subfield in wild-type (*e*, *g*) and TN-C-deficient mice (*f*, *h*). *i–l*, GAD (*i*, *j;* only CA1 subfield shown) and parvalbumin immunoreactivity (*k, l*) showed normal distribution and appearance of GAD- and parvalbumin-positive interneurons in TN-C-deficient mice (*j, l*) when compared with wild-type littermates (*i, k*). *m*, *n*, Immunohistochemistry of WFA lectin-binding sites showing the interneuron-enwrapping perineuronal nets in the CA1 region of wild-type (*m*) and TN-C-deficient (*n*) mice. They were not detectably altered in the mutant. *o*, *p*, The morphology of dendrites and spines of hippocampal pyramidal cells of wild-type (*o*) and TN-C-deficient animals (*p*), visualized with the Golgi method, is indistinguishable between genotypes. Scale bars: (shown in *b*) *a, b,* 25 μm; (shown in *d*) *c, d,* 50 μm; (shown in *j*) *i, j,* 25 μm; (shown in *l*) *e–h, k, l,* 50 μm; (shown in *n*) *m, n,* 25 μm; (shown in *p*) *o, p,* 5 μm.

tected reduced perisomatic inhibition of CA1 pyramidal cells by GABAergic interneurons in mutant mice deficient in the closely related ECM glycoprotein TN-R. To elucidate the distribution and appearance of interneurons and their enwrapping perineuronal nets in TN-C-deficient mutants, we analyzed GAD (Fig. 4, compare *i*, *j*), parvalbumin (Fig. 4, compare *k*, *l*), and WFA (Fig. 4, compare *m*, *n* for CA1 region) immunoreactivity in comparison to wild-type littermates. No significant differences between TN-C-deficient mice and wild-type littermates were detectable. Additionally, examination of Golgi preparations revealed a normal appearance of dendrites and spines of hippocampal pyramidal cells (Fig. 4, compare *o*, *p*). Thus, the lack of TN-C did not detectably affect the histoarchitecture of the murine hippocampus.

Unaltered performance in the water maze task

The protocol of the water maze used to evaluate our mutant was designed such that TN-C-deficient mice and wild-type littermates were tested under conditions (visible platform, hidden platform acquisition, and relearning) that either do or do not implicate the hippocampal formation in solving the task. In particular, the "trial-to-criterion" protocol was designed in a way that the memory of earlier platform locations would interfere with the learning of new locations. Therefore, the most recently encoded location should be selectively retrieved time by time, a characteristic feature of "episodic-like memory," which has been shown to be hippocampus dependent (Aggleton and Brown, 1999; Wood et al., 2000). The performance of TN-C-deficient mice and wild-type littermates in the water maze indicated that both genotypes quickly and reliably learned to locate the platform under all conditions. No difference between genotypes was observed for any of the parameters analyzed during the "visible platform," "acquisition," "relearning," and "training-to-criterion" phases. Thus, TN-C-deficient mice showed apparently normal hippocampus-dependent and hippocampus-independent learning and memory as far as assessed in the water maze with the protocol conducted.

Wild-type and TN-C-deficient littermate mice both swam normally and climbed successfully onto the escape platform in the pool. Performance in the initial visible platform phase revealed no sensorimotor or motivational abnormalities. Mice from both

genotypes quickly reached average escape latencies of <10 sec (Fig. 5*a*). The ANOVA analysis for repeated measure of escape latency, distance moved, velocity, and minimal distance to the wall (thigmotaxis) as analyzed for the visible platform, acquisition, and relearning did not show any effect of genotype and interaction between genotype and trials. As an index for the use of a spatial strategy during the acquisition and relearning phases, the percentage of time spent in five different areas in the arena was analyzed (see Fig. 5*e* for a description of the arena). Both genotypes showed a clear preference for the area surrounding the platform as compared with the chance levels of 10% as well as compared with the percentage of time spent in the other four equivalent areas (data not shown). It is interesting to note that during the relearning phase, mice from both genotypes continued to show a preference for the area where the platform was located during the acquisition phase. During a 60 sec probe trial at the end of the acquisition phase, mice from genotypes spent a significantly higher percentage of time in the area surrounding the northeast (NE) platform location (see Fig. 10*b*). Mutants and wild-type mice spent more time than the chance level also in the northwest (NW) area, which may be attributable to the fact that the starting position during this trial was in the west side of the arena. Indeed, no preference for this area was observed during the acquisition phase. As shown in Figure 5*c*, during the probe trial after the relearning [starting position from the south (S)], both TN-C-deficient and control mice showed a preference for the area surrounding the platform position (NW) as well as for the position of the platform in the former acquisition phase (NE).

It is known that searching strategies and swimming paths are of paramount importance when evaluating the performance of mice in the water maze (Lipp and Wolfer, 1998). Because during the second probe trial TN-C-deficient mice spent more time in the five analyzed areas (NW, NE, E, S, SW) as compared with wild-type littermates ($p = 0.007$), we tested whether there was a different searching strategy used by TN-C-deficient mice and wild-type littermates. Therefore, we analyzed the time spent in an imaginary ring including the area around the platform position during relearning (NW). No difference was found in the time spent in this ring between genotypes ($p > 0.1$). We also analyzed total distance moved, mean velocity, mean distance to the wall, annulus crossing, absolute turning angle, and absolute turning velocity during the probe trials performed after learning and relearning. No difference was found between TN-C-deficient mice and wild-type littermates (data not shown), indicating that TN-C mutants and wild-type mice used indistinguishable searching strategies.

In the training-to-criterion task, both genotypes reached the criterion on an average of seven trials for the first and second platform locations and decreased to five trials for the third one (three being the possible minimum number of trials to reach the criterion) (Fig. 5*d*). The percentage of time spent in different areas during the first trial with a new platform location was used to check whether the animals showed a preference for the area surrounding the platform location of the previous day. Both TN-C-deficient and wild-type mice showed a clear preference for the last platform location and, to a lesser extent, for the second to last platform location (data not shown), showing not only that they used navigation to search for the platform, but that they could also retain the memory trace over a long period of old spatial information.

Impaired TBS-induced LTP in the CA1 region

Stimulus–response curves for fEPSPs evoked by stimulation of Schaffer collaterals and paired-pulse facilitation measured at interpulse intervals between 10 and 200 msec were not different between TN-C-deficient mutants and wild-type littermates, demonstrating normal basal levels of excitatory transmission and its presynaptic modulation in the case of constitutive TN-C deficiency (Fig. 6*a*,*b*). Furthermore, we investigated hippocampal synaptic plasticity in TN-C-deficient mice, starting with the most widely studied form of plasticity, LTP in the CA1 region. TBS of Schaffer collaterals reliably produced short-term potentiation (STP) and LTP in all slices measured from 1-month-old wild-type animals (Fig. 6*c*). The mean level of STP measured as maximal potentiation during 1 min after TBS was 191.1 ± 14.2%, and the level of LTP seen 50–60 min after TBS was 148 ± 4.0%. The levels of STP in 1-month-old TN-C-deficient mice (167.3 ± 8.0%) were not significantly different, whereas TBS-induced LTP was significantly reduced (119.3 ± 3.0%) (Fig. 6*c*,*e*), as compared with wild-type mice. To analyze whether the deficit in LTP was age dependent, we recorded LTP in 3-month-old TN-C-deficient mice and their wild-type control littermates. Again, no significant difference in STP was revealed, whereas LTP was significantly impaired in TN-C mutants (Fig. 6*c*,*e*).

Abolished low-frequency stimulation-induced LTD in the CA1 region

Another NMDA receptor-dependent form of long-term plasticity in the CA1 region is LTD that can be evoked by two trains of low-frequency stimulation (LFS) delivered within a 10 min interval. During LFS, a transient facilitation was observed with similar levels of facilitation and time course for both wild-type and TN-C-deficient mice (Fig. 6*d*, indicated by *1 Hz*). Transient STD followed the facilitation. The mean level of STD (measured as the maximal depression during 1 min after the second LFS) was significantly lower in mutants (reduction to 68.8 ± 3.7% from 100%) than in wild-type animals (reduction to 51.1 ± 3.5% from 100%) (Fig. 6*f*). Long-term reduction of the fEPSP slope by >15% was seen in seven of eight slices prepared from wild-type mice. On average, fEPSP slopes were reduced 50–60 min after induction of LTD by 28.0 ± 5.5% (Fig. 6*d*). In TN-C-deficient mice, the reduction was not larger than by 12% (Fig. 6*f*). The mean slope of fEPSPs measured 50–60 min after the second LFS was close to the baseline level (100.6 ± 3.5%) (Fig. 6*d*). Thus, STD is reduced and LTD is abolished in TN-C-deficient mice.

Normal HFS-induced LTP in the CA3 region

To investigate the regional specificity of abnormalities in synaptic plasticity of the TN-C-deficient hippocampus, LTP at mossy fiber synapses in the CA3 region was particularly interesting to study, because it shows features clearly distinct from CA1 LTP and LTD, being independent of postsynaptic NMDA receptors, mediated by cAMP, and activated by adenylate cyclase and PKA (Weisskopf et al., 1994). Field EPSPs evoked in CA3 pyramidal cells by mossy fiber stimulation are known to be fast and to exhibit paired-pulse facilitation and potentiation during 0.33 Hz stimulation. These criteria were taken to search for responses that were further characterized pharmacologically using L-CCG1, an agonist of type II metabotropic glutamate receptors, which is known to reduce synaptic transmission in CA3 mossy fiber synapses (Maccaferri et al., 1998; Eckhardt et al., 2000).

Low-frequency stimulation (0.33 Hz) potentiated fEPSPs to ~250% in wild-type and TN-C mutant mice (Fig. 7*a*). L-CCG1

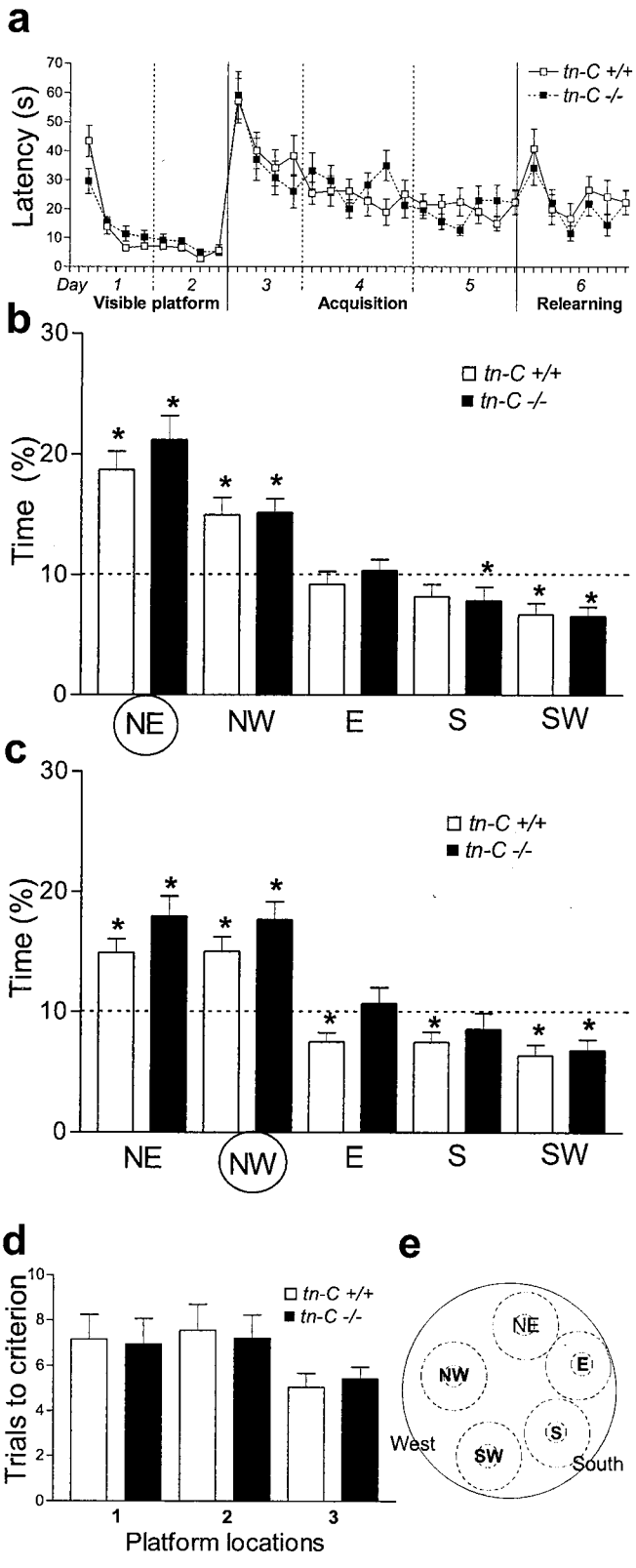

Figure 5. Unaltered learning, spatial memory, and relearning of TN-C-deficient mice. *a*, Latencies to climb the platform during the visible platform task, the spatial learning acquisition, and the relearning. Each value represents one trial (mean ± SEM). Mice from both genotypes quickly learned to locate the platform in all three phases. *b*, During the probe trial at the end of the acquisition phase, both genotypes showed a preference for the area surrounding the platform in *NE*. The preference for the area in *NW* might be attributable to the fact that animals were started from the west (mean ± SEM). *c*, After five trials with the platform located at a new position (*NW*), both genotypes showed a preference for the area around the platform location (*NW*) as well as for the area where the platform was located during the former acquisition phase (*NE*). *Asterisks* indicate a difference to the chance level of 10% at a significance of $p < 0.005$ (Wilcoxon signed rank test; mean ± SEM). *d*, The analysis of the number of trials needed to reach criterion for three successive platform locations during the trial-to-criterion task (days 7–12) revealed no difference between genotypes (mean ± SEM). *e*, Scheme of the circular water maze (diameter, 155 cm) with different platform locations (platform diameter, 14 cm) surrounded by a circular area equal to 10% of the total area of the maze.

similarly diminished the amplitude of fEPSPs in both genotypes (Fig. 7*b*). The NMDA receptor antagonist AP-5 did not affect the amplitude of selected fEPSPs in either wild-type or TN-C mutant mice (Fig. 7*c*). HFS performed in the presence of AP-5 induced a strong increase in fEPSP amplitudes (Fig. 7*c*). Post-tetanic potentiation (PTP) during the first 1 min after HFS was ~900%, and mean potentiation measured 50–60 min after induction of LTP was ~200%, resembling reported profiles of LTP in CA3 in mice (Maccaferri et al., 1998; Eckhardt et al., 2000). There was no difference between wild-type littermate and TN-C mutant mice in PTP or LTP (Fig. 7*c–e*).

To verify that we analyzed PKA-dependent mossy fiber LTP, HFS was applied after incubation and perfusion of slices from wild-type mice with the PKA antagonist Rp-cAMPS. This treatment strongly diminished both PTP (411.8 ± 38.8%) and LTP (115.1 ± 9.6%) of the recorded fEPSP (Fig. 7*c*). We conclude that NMDA receptor-independent, PKA-mediated LTP in mossy fiber–CA3 synapses is normal in TN-C-deficient mutants.

Normal HFS-induced LTP in the dentate gyrus

To complete the analysis of the trisynaptic circuit in the hippocampus, we recorded NMDA receptor-dependent LTP in the synapses formed by the medial and lateral perforant pathways in the dentate gyrus. The fEPSPs evoked by paired-pulse stimulation of the medial perforant pathway (with a 50 msec interval) exhibited paired-pulse depression independently of the genotype (79.9 ± 5.9%, $n = 7$ in TN-C-deficient mice and 86.6 ± 4.4%, $n = 8$ in wild-type littermates). Paired-pulse stimulation of the lateral perforant pathway elicited facilitation of similar magnitude in both TN-C-deficient (124.4 ± 4.8%; $n = 8$) and wild-type (122.5 ± 5.9%; $n = 6$) mice. SHFS applied in the presence of the $GABA_A$ receptor antagonist picrotoxin induced similar levels of LTP in the slope of fEPSPs measured 50–60 min after stimulation. SHFS of the medial perforant pathway potentiated the slope of EPSPs to 135.1 ± 5.1% in wild-type mice and 134.0 ± 4.0% in TN-C-deficient mutants (Fig. 8*a*,*c*). SHFS of the lateral perforant pathway potentiated the slope of EPSPs to 135.4 ± 9.8% in TN-C-deficient mice and 137.1 ± 7.9% in wild-type littermates (Fig. 8*b*,*d*). Thus, there was no difference between genotypes in synaptic plasticity in the lateral and medial perforant path connections to the dentate gyrus.

Reduced LTP in the CA1 region of TN-C-deficient mice is not caused by increased levels of inhibition or impaired NMDA receptor-mediated transmission

Because LTP recorded in the dentate gyrus of TN-C mutants in the presence of picrotoxin was normal and abnormal levels of perisomatic inhibition had been revealed in mice deficient

←

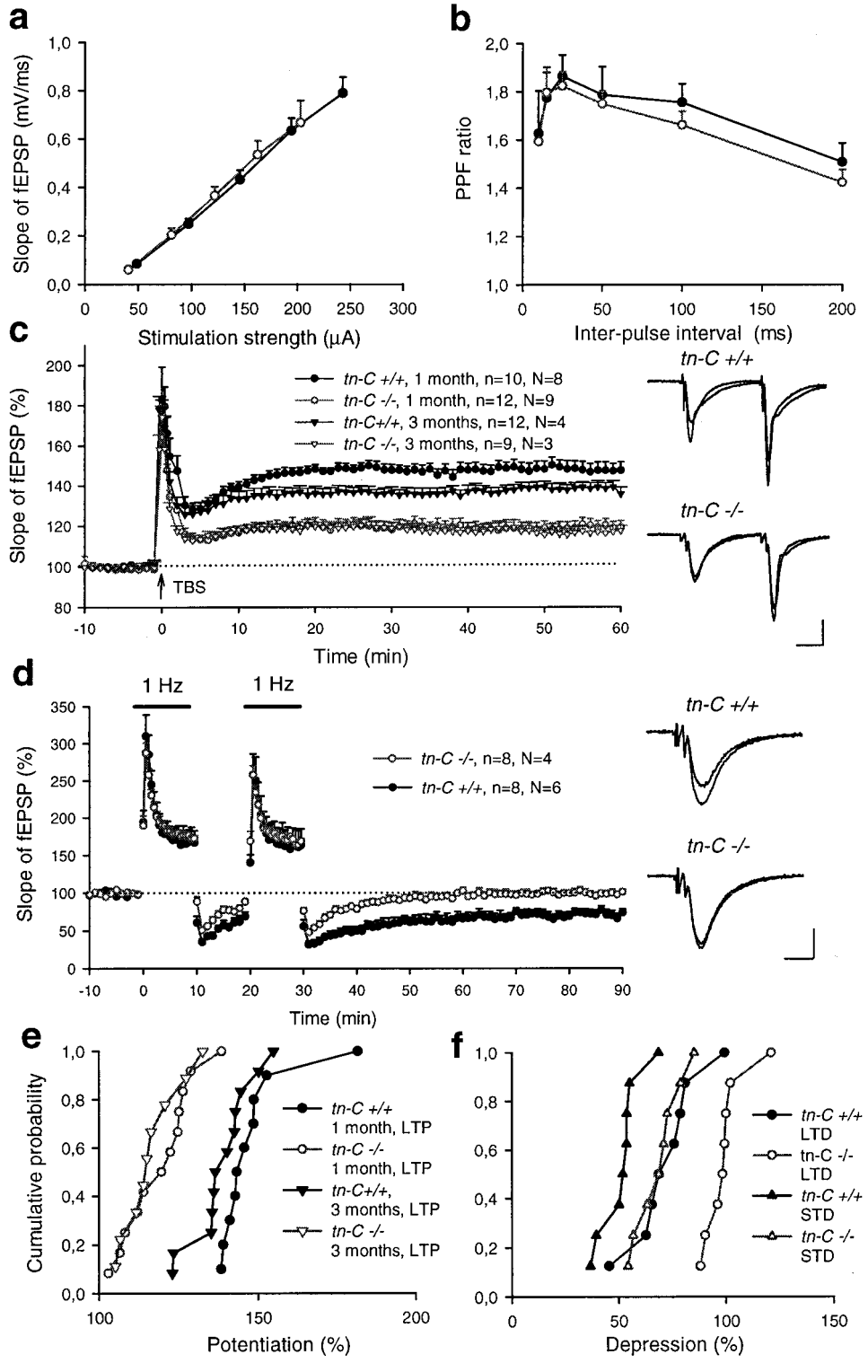

Figure 6. LTP and LTD in the CA1 region are impaired in TN-C-deficient mice. *a*, Input–output curves for slopes of fEPSPs evoked by stimulation of Schaffer collaterals at different stimulation strengths. No significant difference between genotypes was found. *b*, Paired-pulse facilitation (*PPF*) was measured as the ratio between the slopes of fEPSPs evoked by the second and first pulses and plotted for several interpulse intervals. Field EPSPs were recorded at 30% from the subthreshold strength. To measure slopes of overlapping fEPSPs evoked by paired-pulse stimulation (for interpulse intervals <50 msec), fEPSPs evoked by a single-pulse stimulation were subtracted from fEPSPs evoked by paired-pulse stimulation. Examples of fEPSPs evoked by paired-pulse stimulation are shown in *c*, *right panels*. No significant difference between genotypes was found. *c*, TBS of Schaffer collaterals (applied at time point 0) evoked a high increase in the slopes of fEPSPs recorded in the CA1 region of slices from wild-type mice. In slices from TN-C-deficient mice (*tn-C* −/−), the potentiation appeared lower than in wild-type mice (*tn-C* +/+). The mean slope of fEPSPs recorded 0–10 min before TBS was taken as 100%. Data represent mean + SEM; *n* indicates the number of tested slices; *N* indicates the number of tested mice. *Right panels* show fEPSPs recorded before and 60 min after TBS. Scale bars, 20 msec and 500 μV. *d*, Two trains of low-frequency stimulation (1 Hz, indicated by *horizontal bars*) of Schaffer collaterals reliably decreased the slopes of fEPSPs in slices from wild-type mice (*tn-C* +/+). In slices from TN-C-deficient mice (*tn-C* −/−), the slope returned to the baseline. The mean slope of fEPSPs recorded 10 min before the first train was taken as 100%. Data represent mean + SEM; *n* indicates the number of tested slices; *N* indicates the number of tested mice. *Right panels* show fEPSPs in TN-C-deficient (*tn-C* −/−) and wild-type (*tn-C* +/+) mice before and 60 min after induction of LTD. Calibration: 10 msec, 500 μV. *e*, Cumulative plots representing levels of STP and LTP from all experiments. Each *symbol* represents a single experiment. Cumulative probability at any given value *X* is the probability to observe potentiation less than or equal to *X*. Lower values of LTP (there is no overlap of values measured in young *tn-C* −/− and *tn-C* +/+ mice) are evident for TN-C-deficient mutants when compared with wild-type littermates. *f*, Cumulative plots representing levels of STD and LTD from all experiments. Each *symbol* represents a single experiment. Cumulative probability at any given value *X* is the probability to observe depression less than or equal to *X*. Lower values of both STD and particularly LTD are evident for TN-C mutants when compared with wild-type littermates.

for the closely related tenascin family member TN-R (Saghatelyan et al., 2001), we hypothesized that TN-C mutants could have elevated levels of $GABA_A$ receptor-mediated inhibition impeding induction of LTP in CA1 in the absence of picrotoxin. We therefore recorded CA1 LTP in the presence of picrotoxin with the hope of rescuing LTP in TN-C-deficient mice. Indeed, the average level of LTP in mutants was increased in the presence of picrotoxin to 145.1 ± 4.1%, remaining significantly lower than LTP seen in wild-type littermates after picrotoxin application (167.5 ± 6.2%) (Fig. 9*a*,*c*). These findings indicate that mechanisms distinct from GABAergic inhibition mediate most, if not all, reduction of LTP in TN-C-

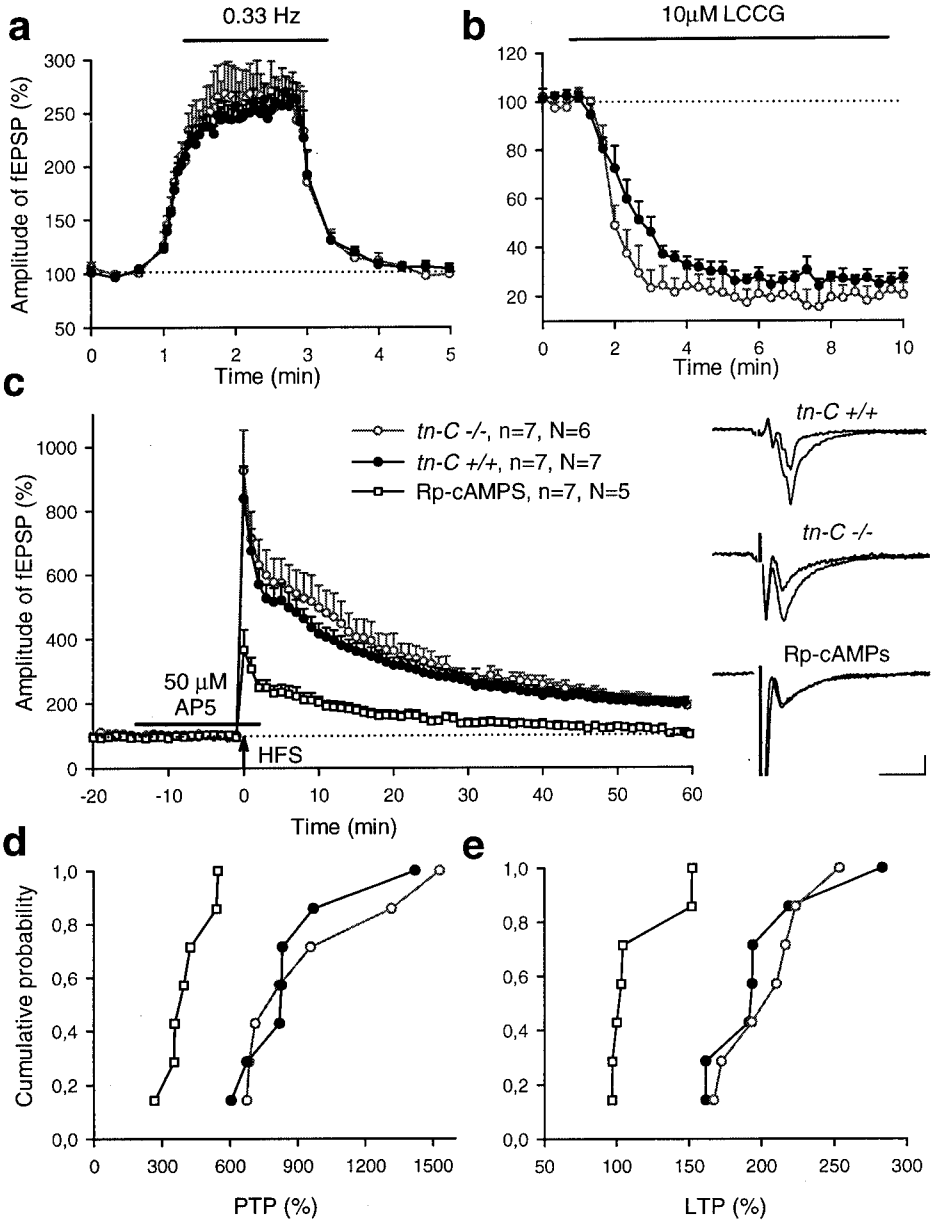

Figure 7. Normal LTP in the CA3 region of TN-C-deficient mice. *a*, Stimulation of mossy fibers with a frequency of 0.33 Hz similarly increased the amplitudes of fEPSPs in acute slices from both TN-C-deficient (*tn-C* −/−) and wild-type (*tn-C*+/+) mice. *b*, Application of the type II metabotropic glutamate receptor agonist L-CCGI (10 μM) reduced the amplitude of fEPSPs in slices from both TN-C-deficient (*tn-C* −/−) and wild-type (*tn-C* +/+) mice to the same level. *c*, High-frequency stimulation (*HFS*) of mossy fibers (applied at time point 0) evoked a similar increase in slopes of fEPSPs in slices from TN-C-deficient (*tn-C* −/−) and wild-type (*tn-C* +/+) mice, respectively. The potentiation was impaired in wild-type slices treated with a competitive inhibitor for PKA, Rp-cAMPS. The time interval of the application of the NMDA receptor antagonist AP-5 is shown by a *horizontal bar*. Mean slope of fEPSPs recorded 0–10 min before HFS was taken as 100%. *Right panels* show averaged fEPSPs recorded before and 60 min after induction of LTP in TN-C-deficient (*tn-C* −/−) and wild-type (*tn-C* +/+) mice. Calibration: 10 msec, 100 μV. *d*, *e*, Cumulative plots representing levels of PTP (*d*) and LTP (*e*) from all experiments. Each *symbol* represents a single experiment. Cumulative probability at any given value *X* is the probability to observe a potentiation less than or equal to *X*. Note similar values of PTP and LTP in TN-C-deficient (*tn-C* −/−) and wild-type (*tn-C* +/+) mice and that Rp-cAMPS completely blocked LTP in five of seven experiments. 100% corresponds to the baseline level.

deficient mutants. STP values were slightly but not significantly higher in wild-type mice than in mutants (193.0 ± 24.1 vs 172.3 ± 11.3%, respectively) (Fig. 9*a*,*b*).

Another explanation for the reduction of LTP in TN-C-deficient mutants would be an impairment of NMDA receptor-mediated transmission. To estimate the NMDA receptor-dependent component, we computed the difference between fEPSPs evoked by TBS before and after application of the NMDA receptor antagonist AP-5. There was no significant difference in the magnitude of this component between genotypes (5.5 ± 0.8% in wild-type mice vs 6.4 ± 0.6% in TN-C-deficient littermates) (Fig. 9*d*). Levels of potentiation recorded immediately after four trains of TBS in the presence of AP-5 were similar in wild-type (116 ± 12.5%; $n = 10$) and TN-C-deficient mice (118 ± 7.2%; $n = 9$). Thus, impairment of LTP in TN-C-deficient mutants did not appear to be related to increased activity of inhibitory interneurons or reduced function of NMDA receptors during TBS.

Temporal pattern of stimulation and activation of Ca^{2+} channels determines dependency of LTP on TN-C in the CA1 region

A difference in protocols used for the induction of LTP in the CA1 subfield and the dentate gyrus was that in the CA1 region we applied TBS rather than SHFS. The temporal pattern of stimulation is an important parameter that determines, for instance, the neurotrophin dependency of LTP (Kang et al., 1997). To determine whether the impairment in TBS-induced LTP in CA1 in TN-C-deficient mice was region- or induction protocol-specific, we measured LTP at Schaffer collateral–CA1 synapses using exactly the same pattern of stimulation as used in the dentate gyrus. Remarkably, no difference was seen in the levels of LTP between genotypes after application of SHFS (119.3 ± 3.2% in TN-C-deficient mice vs 114.0 ± 3.4% in wild-type littermates) (Fig. 10*a*). Higher levels of LTP were induced by the SHFS protocol in the presence of picrotoxin, but again no significant

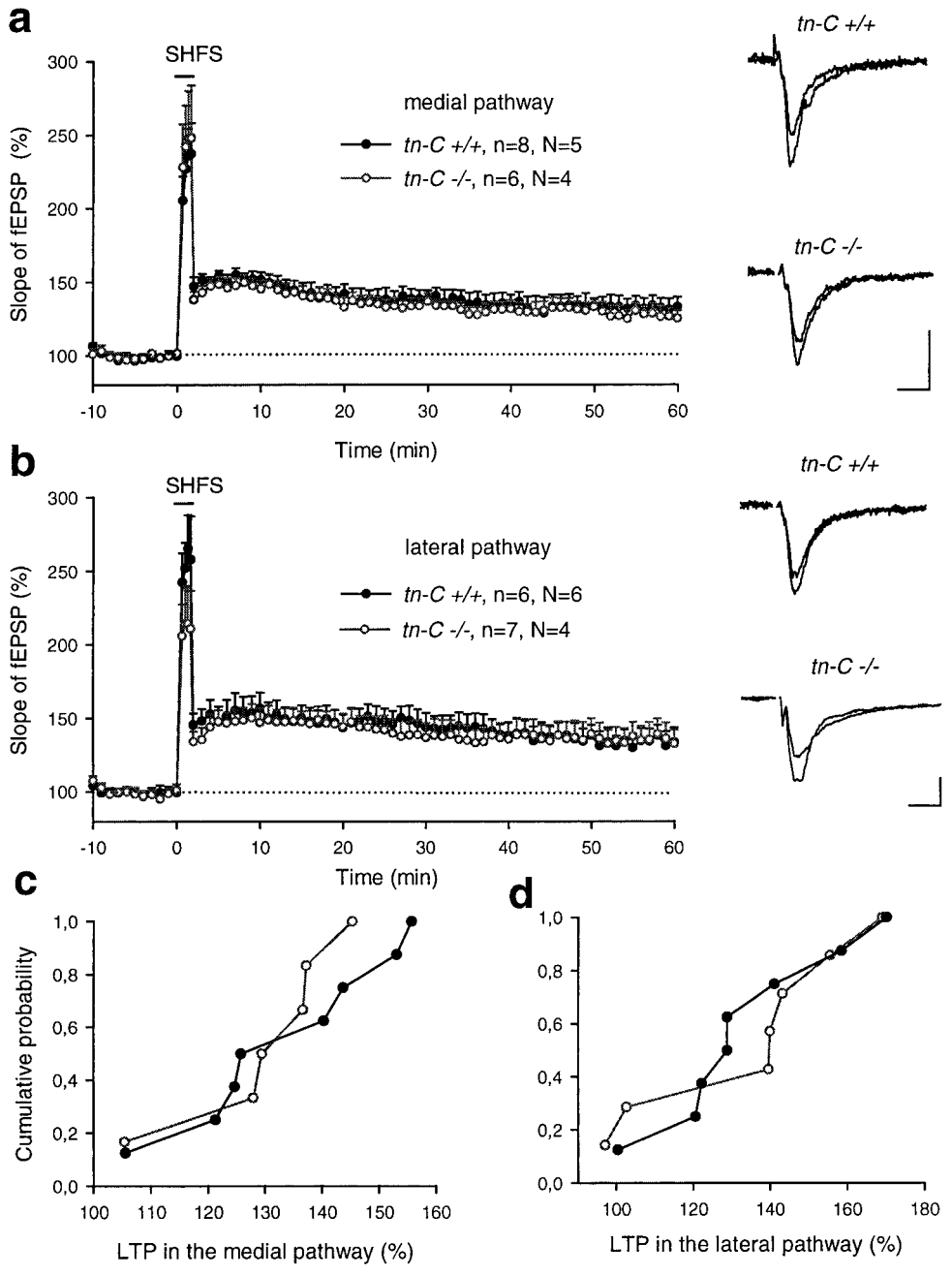

Figure 8. Normal LTP in the dentate gyrus of TN-C-deficient mice. *a*, *b*, Short high-frequency stimulation (*SHFS*) of the medial (*a*) or lateral (*b*) perforant pathway (applied at time point 0) evoked a similar potentiation in slices from wild-type (*tn-C* +/+) and TN-C-deficient mice (*tn-C* −/−) in the presence of 100 μM picrotoxin. Mean slope of fEPSPs recorded 0–10 min before TBS was taken as 100%. Four points recorded during the period marked by SHFS represent potentiation recorded between five trains (10 sec after a train). Data represent mean + SEM; *n* indicates the number of tested slices; *N* indicates the number of tested mice. *Right panels* show fEPSPs recorded before and 60 min after TBS. Calibration: 10 msec, 250 μV. *c*, *d*, Cumulative plots representing levels of LTP measured 50–60 min after beginning of high-frequency stimulation of medial (*a*) or lateral (*b*) perforant pathway. Each *symbol* represents a single experiment. Cumulative probability at any given value *X* is the probability to observe a potentiation less than or equal to *X*. No significant difference between genotypes was found.

difference between genotypes was seen (159.6 ± 8.9%, $n = 4$ in TN-C-deficient mice vs 151.5 ± 5.0%, $n = 5$ in wild-type littermates).

Evidently, TBS is a "stronger" stimulation paradigm than short HFS, both in terms of the number of stimuli (40 vs 10) and the resulting levels of potentiation. It therefore seems that only strong depolarization of postsynaptic cells could activate L-type VDCCs. Indeed, previous studies demonstrated a contribution of these classes of VDCCs during repetitive TBS (Huber et al., 1995; Morgan and Teyler, 2001). Because the NMDA receptor-mediated component of LTP appeared to be normal in TN-C-deficient animals, we investigated the contribution of L-type VDCCs to the differences in LTP found between genotypes. Strikingly, the levels of TBS-induced LTP seen in the presence of nifedipine, an antagonist of L-type VDCCs, were very similar in TN-C-deficient (115.9 ± 3.7%) and wild-type (119.5 ± 5.5%) (Fig. 10*b*) mice. These levels were also close to those observed in TN-C-deficient mice without nifedipine or after induction of LTP by SHFS in either genotype (Fig. 10, compare *a*, *d*). The latter protocol is apparently L-type VDCC-independent, because LTP could be reliably induced by SHFS in the presence of nifedipine in wild-type mice (125.7 ± 0.6%; $n = 4$; data not shown). Thus, the difference in TBS-induced LTP between genotypes is mediated by a nifedipine-sensitive, L-type VDCC-mediated component, whereas genotypes are not different in the levels of nifedipine-insensitive SHFS-induced LTP.

On the basis of these results, we predicted an impairment of another VDCC-dependent form of synaptic plasticity in TN-C-deficient mice, namely of LTP chemically induced by short-term bath application of the K^+-channel blocker tetraethylammonium

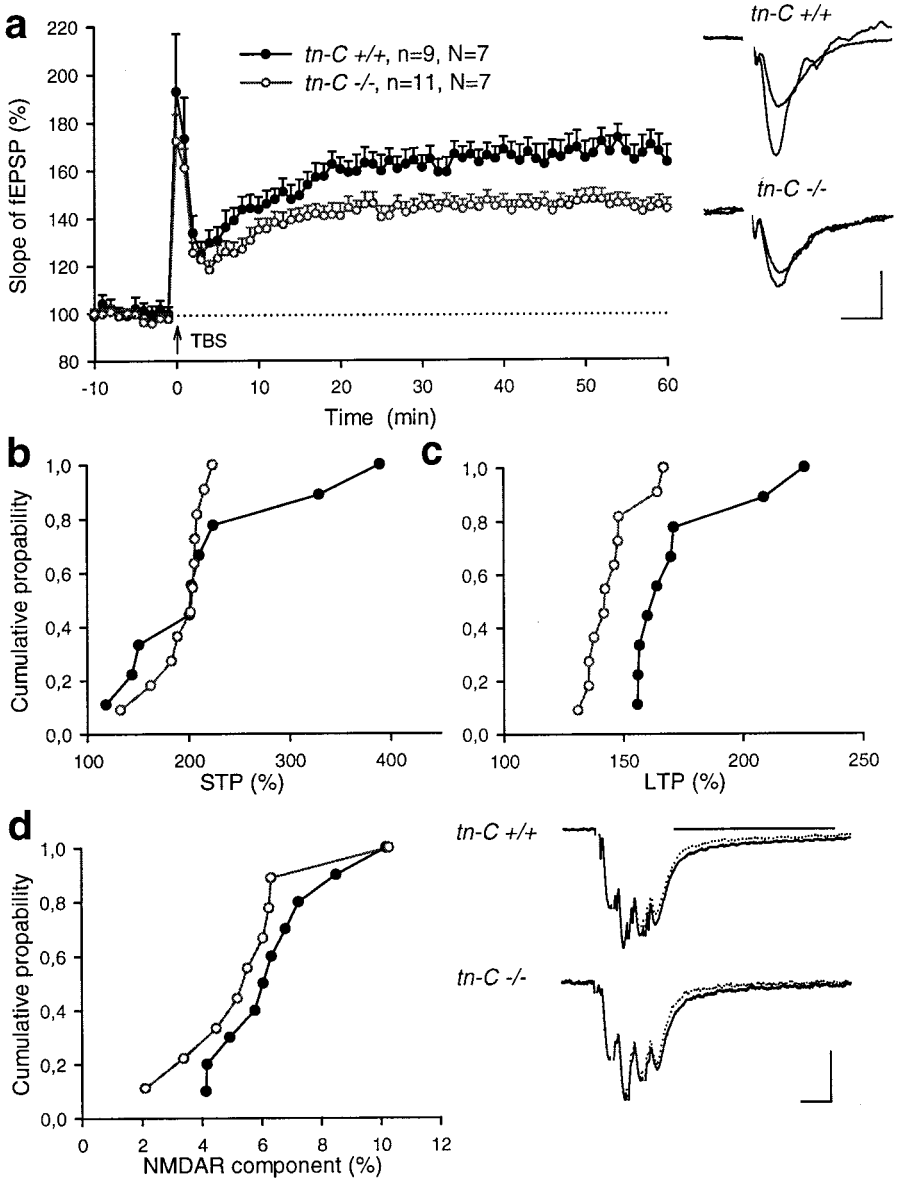

Figure 9. Blockade of $GABA_A$ receptor-mediated inhibition does not fully rescue LTP in the CA1 region of TN-C-deficient mice. *a*, TBS of Schaffer collaterals in the presence of picrotoxin evoked an increase in the slopes of fEPSPs recorded in the CA1 region of slices from wild-type mice (*tn-C* +/+). In slices from TN-C-deficient littermates (*tn-C* −/−), potentiation appeared significantly lower than in wild-type mice. Mean slope of fEPSPs recorded 0–10 min before TBS was taken as 100%. Data represent mean + SEM; *n* indicates the number of tested slices; *N* indicates the number of tested mice. *Right panels* show fEPSPs recorded before and 60 min after TBS. Calibration: 20 msec, 500 μV. *b*, *c*, Cumulative plots represent levels of STP (*b*) and LTP (*c*) from all experiments performed in the presence of picrotoxin. Each *symbol* represents a single experiment. Cumulative probability at any given value *X* is the probability to observe a potentiation less than or equal to *X*. Note the overlap of STP values and significant difference in distribution of LTP levels: 9 of 11 values corresponding to TN-C-deficient mutants are lower than the smallest LTP value for wild-type littermates. *d*, Cumulative plot represents values of the NMDA receptor-mediated component in fEPSPs evoked by single theta bursts. Examples of such fEPSPs recorded without (*solid lines*) or in the presence (*dotted lines*) of the NMDA receptor antagonist AP-5 are shown on the *right*. *Horizontal bar* indicates the time interval used for measurements of the NMDA receptor-mediated component. No significant difference between genotypes was found.

(TEA) (Anikstejn and Ben Ari, 1991; Huang and Malenka, 1993). This treatment reliably evoked LTP in wild-type mice (152.8 ± 9.6%) (Fig. 10*c*,*e*). In agreement with previous reports demonstrating that TEA-induced potentiation is sensitive to nifedipine (Anikstejn and Ben Ari, 1991; Huang and Malenka, 1993), this type of potentiation was also strongly diminished by nifedipine under our conditions (115.0 ± 8.9%; $n = 5$; data not shown). Similar levels of potentiation were seen during application of TEA to slices from TN-C-deficient animals. However, the levels of LTP recorded 50–60 min after washout of TEA were much lower in TN-C mutants (126.6 ± 5.5%) than in wild-type mice (152.8 ± 9.6%). Thus, two forms of VDCC-dependent LTP, induced by either TBS or TEA application, were impaired in constitutively TN-C-deficient mice.

DISCUSSION

We transiently expressed Cre recombinase in ES cells harboring a floxed *tn-C* allele to generate a constitutively TN-C-deficient mouse. This mutant lacks detectable levels of TN-C protein or a truncated form thereof as judged from immunoblot experiments that revealed <0.05% of the amount of TN-C protein normally expressed in wild-type mice. Constitutively TN-C-deficient mice showed no apparent morphological abnormalities as reported for two previously generated TN-C-deficient mice (Saga et al., 1992; Forsberg et al., 1996). The gross anatomy of retina, cerebrum, and cerebellum and the distribution of oligodendrocytes in the optic nerve were indistinguishable between genotypes. Furthermore, there were no ultrastructural abnormalities of myelin and the cerebellum.

Impaired synaptic plasticity as a result of TN-C deficiency

Because TN-C in the hippocampus is expressed in the hippocampus in an activity-dependent manner (Nakic et al., 1996, 1998) and synaptic plasticity has not been studied previously in TN-C-deficient mice, we investigated hippocampal histoarchitecture, synaptic efficacy, and hippocampus-dependent learning and memory in our mutant. Morphologically, the hippocampus appeared indistinguishable between genotypes. CA1 through CA3 regions, including mossy fiber projections, the laminated organization in

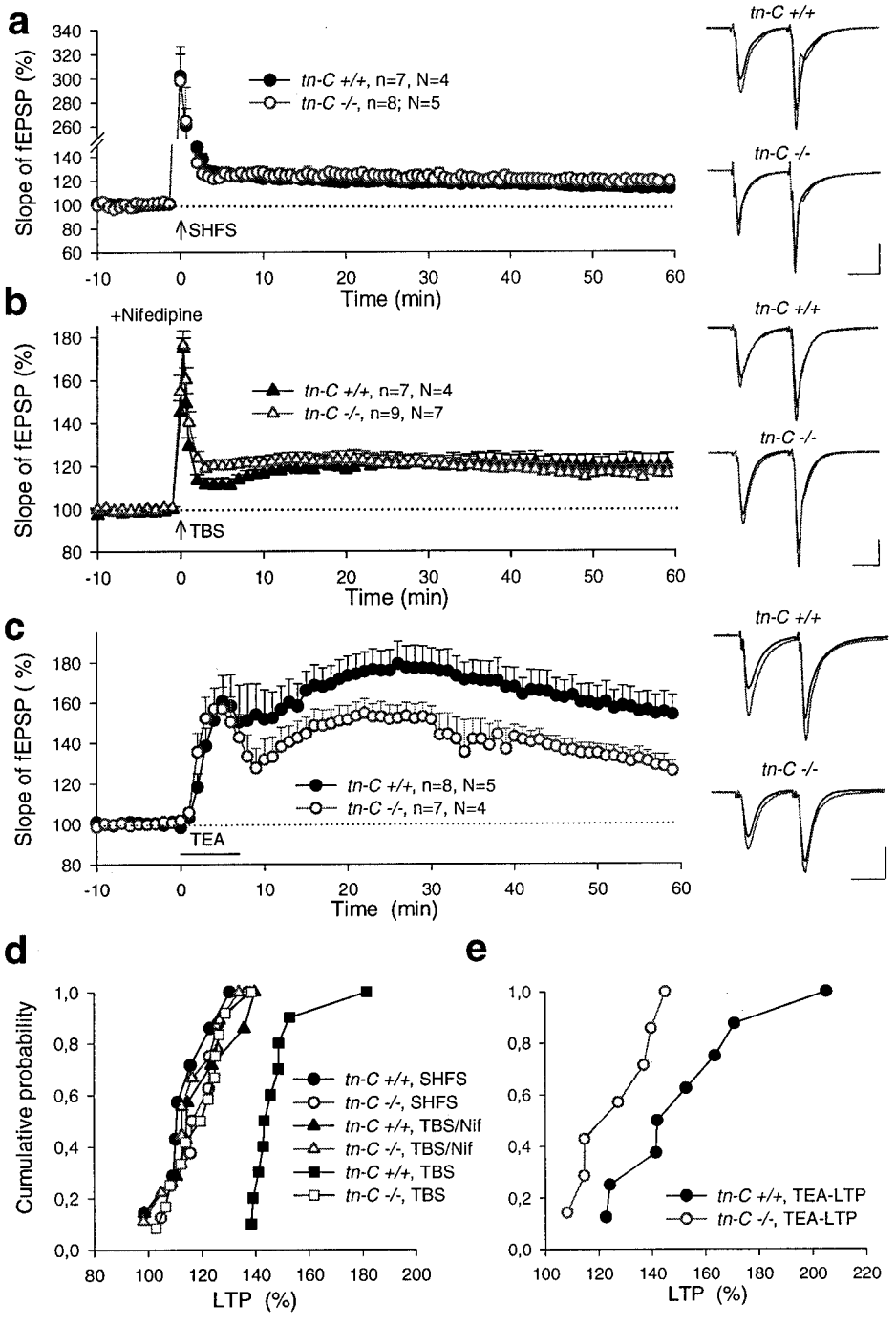

Figure 10. Voltage-dependent Ca^{2+} channels mediate deficits in synaptic plasticity in TN-C-deficient mutants. *a*, *b*, Short high-frequency stimulation (*SHFS*) in normal ACSF (*a*) or theta-burst stimulation (*TBS*) in the presence of 20 μM nifedipine (*b*) applied at time point 0 evoked a similar potentiation in the CA1 region in wild-type (*tn-C* +/+) and TN-C-deficient (*tn-C* −/−) mice. Four points recorded during the period marked by *SHFS* represent potentiation recorded among five trains (10 sec after a train). *c*, Bath application of 25 mM tetraethylammonium (applied at time point 0 for 7 min) evoked stronger LTP in the CA1 region of wild-type (*tn-C* +/+) as compared with TN-C-deficient (*tn-C* −/−) mice. In *a–c*, mean slope of fEPSPs recorded 0–10 min before TBS was taken as 100%. Data represent mean + SEM; *n* indicates the number of tested slices; *N* indicates the number of tested mice. *Right panels* show fEPSPs recorded before and 60 min after induction of LTP. Calibration: 10 msec, 500 μV. *d*, *e*, Cumulative plots representing levels of LTP measured 50–60 min after induction of LTP according to protocols given in *a* and *b* (*d*) and *c* (*e*), respectively. To facilitate comparison of experiments performed in the presence and absence of nifedipine (*Nif*), data presented in Figure 6*e* for young mice are added to *d*. Each *symbol* represents a single experiment. Cumulative probability at any given value *X* is the probability to observe LTP less than or equal to *X*.

the latter region, and the dentate gyrus were apparently normal. Despite the normal hippocampal histoarchitecture and a wild-type-like performance of TN-C-deficient mice in the water maze, we found selective impairments of several forms of synaptic plasticity in acute slices from TN-C mutants. Specifically, TBS-induced LTP was reduced at Schaffer collateral–CA1 synapses. Basal synaptic activity was unaffected, but LFS-induced STD was impaired and LTD was abolished at these synapses. Combined with our previous observations that altered synaptic activity changes expression of TN-C in the hippocampus (Nakic et al., 1996, 1998), it is conceivable that a feedback-loop exists between synaptic plasticity that depends on TN-C expression and the upregulation of TN-C after induction of increased synaptic activity. Whether these alterations in synaptic efficacy are caused by subtle alterations of synapses during development or acute action of TN-C on normally developed synapses remains to be elucidated by using conditionally deficient TN-C mutants. Our recent observations that injection of TN-C fragments (fibronectin type III domains 6–8 but not domains 3–5) into the CA1 region of acute hippocampal slices from wild-type mice reduced LTP argue in favor of a direct involvement of TN-C in synaptic plasticity (Strekalova et al., 2002).

Impairment of L-type VDCC-dependent LTP and LTD at Schaffer collateral–CA1 synapses

Both LTP and LTD at Schaffer collateral–CA1 synapses depend on NMDA receptors and VDCCs (Bolshakov and Siegelbaum,

1994; Huber et al., 1995; Christie et al., 1997; Morgan and Teyler, 2001). These two possible sources of Ca^{2+} entry appear to activate different signal transduction pathways because antagonists of serine–threonine kinases inhibit NMDA receptor-dependent LTP, whereas antagonists of tyrosine kinases inhibit VDCC-dependent LTP (Cavus et al., 1996). We examined TBS-induced LTP in the CA1 region using a stimulation protocol very similar to that reported to activate L-type VDCCs (Morgan and Teyler, 2001). Consistently, nifedipine, an antagonist of these Ca^{2+} channels, reduced TBS-induced LTP in wild-type mice. LTP was reduced to levels comparable to those of TBS-induced LTP in TN-C-deficient littermates without previous blocking of L-type VDCCs, suggesting that mainly an L-type VDCC-specific component of LTP at Schaffer collateral–CA1 synapses is diminished in the mutant. LTP induced by the K^+ channel blocker TEA in CA1 is another form of synaptic plasticity that is dependent on the activation of L-type VDCCs [Huang and Malenka (1993); but see also Song et al. (2001)]. Reduced TEA-induced LTP in TN-C-deficient animals further supports the view that L-type VDCCs or L-type VDCC-mediated signaling events are impaired. Involvement of these channels in LTD at Schaffer collateral–CA1 synapses is also well documented (Bolshakov and Siegelbaum, 1994; Christie et al., 1997). Interestingly, LTD is abolished in TN-C-deficient mice, underscoring the idea that TN-C-dependent plasticity is mediated by L-type VDCCs. Furthermore, LTP induced by SHFS, i.e., under rather "weak" induction conditions, resulted in L-type VDCC-independent LTP. Consistently, we found no difference in SHFS-induced LTP in the CA1 region between genotypes.

LTP in the dentate gyrus and the CA3 region was investigated to complete the electrophysiological analysis of the trisynaptic circuit in TN-C-deficient mice. Paired-pulse modulation and SHFS-induced LTP were normal in the medial and lateral perforant path–granule cell synapses in the dentate gyrus. The VDCC dependency of this synapse plasticity is, to our knowledge, not entirely understood. L-type VDCCs appear not to be critically involved in this particular form of LTP induced by the weak stimulation protocol. In the CA3 region, we used the stimulation protocol that has been reported to induce L-type VDCC-independent LTP (Kapur et al., 1998). Consistently with this, we observed normal CA3 LTP in TN-C-deficient mice. The dependence of CA3 LTP evoked by stronger stimulation protocols on postsynaptic entry of Ca^{2+} via L-type VDCCs has been debated (Kapur et al., 1998; Mellor and Nicoll, 2001). Recent data point to the involvement of non-L-type Ca^{2+} channels in CA3 LTP (Heinz Beck, personal communication). The combined observations support the view that deficits in synaptic plasticity in TN-C-deficient mice are observed exclusively under conditions involving activation of L-type VDCCs.

TN-C and L-type VDCCs in spatial learning and memory

Encoding of spatial information is hippocampus dependent (Morris et al., 1982; Shapiro and Eichenbaum, 1999). In rodents, the hippocampus has also been shown to be involved in the formation of episodic-like memory (Aggleton and Brown, 1999; Wood et al., 2000). In the present study, the integrity of both reference and working/episodic-like memory capabilities of TN-C-deficient mice was demonstrated in the water maze following a trial-to-criterion protocol as described by Chen et al. (2000). It has been postulated that hippocampal LTP is linked to long-term memory storage and episodic-like memory (Miller and Mayford, 1999; Kesner and Rolls, 2001). Particularly, levels of NMDA receptor-dependent LTP at Schaffer collateral-A1 synapses have been correlated with performance in certain tests of spatial learning and memory (Tsien et al., 1996; Shimizu et al., 2000; Zeng et al., 2001). However, such a correlation has been controversial (Cain, 1997; Shors and Matzel, 1997). Several studies on transgenic animals describe a dissociation of certain aspects of spatial learning and memory from hippocampal NMDA receptor-dependent LTP (Saucier and Cain, 1995; Zamanillo et al., 1999).

To our knowledge, the present study is the first to describe a mouse mutant showing a dissociation of impaired levels of L-type VDCC-dependent hippocampal plasticity at Schaffer collateral–CA1 synapses from spatial learning and memory, including episodic-like memory, as assessed in the water maze. Chronic or acute treatment of young wild-type mice with L-type VDCC antagonists failed to show a functional role of these channels in spatial learning in the water maze (Riekkinen et al., 1997). However, experiments addressing the role of L-type VDCCs in learning and memory have shown ambiguous results. Although some studies have shown an impairment of spatial learning (Maurice et al., 1995), others described either an improvement of the performance (McMonagle-Strucko and Fanelli, 1993; Quartermain et al., 2001) or no effect of a pretraining treatment with L-type VDCC antagonists (Riekkinen et al., 1997). Contradictory results have also been reported in other learning paradigms, including passive avoidance or visual discrimination in chicken. Discrepancies have been explained, for instance, by inverted U-shaped dose–response curves (Quevedo et al., 1998).

Different protocols have been used to study LTP. However, it is often not clear whether and to what extent L-type VDCCs have been activated or coactivated with NMDA receptors in these experiments. The detailed analysis of L-type VDCC- and NMDA receptor-dependent components of hippocampal synaptic plasticity in mutant mice, which display dissociation of LTP and spatial learning and memory in the water maze, could help to evaluate a more general validity of our findings in TN-C-deficient mice. Such studies would resolve the role of L-type VDCC-dependent plasticity in spatial learning and memory.

TN-C and L-type VDCCs: direct interaction or indirect interplay?

In most tissues, cells are embedded in a network of extracellular macromolecules, such as heparin-binding growth-associated molecule, TN-R, and laminin, which have been implicated in synaptic plasticity (Lauri et al., 1998; Saghatelyan et al., 2000, 2001; Zhou et al., 2001). TN-C may modulate L-type VDCC-dependent synaptic plasticity by interaction with its cellular receptors, different types of integrins (Jones and Jones, 2000), or other extracellular binding partners. For instance, chondroitin proteoglycans, which interact with TN-C (Milev et al., 1997), can bind to Na^+ channels (Ratcliffe et al., 2000) and regulate Ca^{2+} entry via voltage-independent Ca^{2+} channels in growth cones (Snow et al., 1994). Abolishment of LTD in the CA1 region of hippocampal slices by removal of chondroitin sulfates with chondroitinase ABC (Bukalo et al., 2001) might be related to these interactions. It is interesting that the α subunits of the voltage-dependent Ca^{2+} and Na^+ channels are structurally similar (Anderson and Greenberg, 2001). Because TN-C is known to interact with voltage-dependent Na^+ channels (Srinivasan et al., 1998) [for TN-R, see also Davis et al. (2001)], we favor the possibility that TN-C might directly affect L-type VDCCs.

In conclusion, our study instigates interest in the mechanism by

which TN-C acts on L-type VDCC-mediated currents and signaling. Furthermore, because several studies have shown an involvement of L-type VDCCs in age-associated neurodegeneration and learning impairments (Sandin et al., 1990; Thibault and Landfield, 1996; Thibault et al., 2001), it will be important to test spatial learning and memory in aged TN-C-deficient mice. Our study also suggests that an analysis of NMDA receptor- and L-type VDCC-dependent components of synaptic plasticity in the trisynaptic circuit of the hippocampus of different mutant mice in conjunction with spatial learning and memory tests would be an exciting attempt to merge electrophysiological and behavioral data into a more coherent picture of learning-induced synaptic plasticity.

REFERENCES

Aggleton JP, Brown MW (1999) Episodic memory, amnesia, and the hippocampal-anterior thalamic axis. Behav Brain Sci 22:425–444.

Anderson PA, Greenberg RM (2001) Phylogeny of ion channels: clues to structure and function. Comp Biochem Physiol B Biochem Mol Biol 129:17–28.

Andrews BJ, Proteau GA, Beatty LG, Sadowski PD (1985) The FLP recombinase of the 2 micron circle DNA of yeast: interaction with its target sequences. Cell 40:795–803.

Anikszteyn L, Ben Ari Y (1991) Novel form of long-term potentiation produced by a K+ channel blocker in the hippocampus. Nature 349:67–69.

Bartsch S, Bartsch U, Dorries U, Faissner A, Weller A, Ekblom P, Schachner M (1992) Expression of tenascin in the developing and adult cerebellar cortex. J Neurosci 12:736–749.

Bartsch U (1996) The extracellular matrix molecule tenascin-C: expression in vivo and functional characterization in vitro. Prog Neurobiol 49:145–168.

Bartsch U, Faissner A, Trotter J, Dorries U, Bartsch S, Mohajeri H, Schachner M (1994) Tenascin demarcates the boundary between the myelinated and nonmyelinated part of retinal ganglion cell axons in the developing and adult mouse. J Neurosci 14:4756–4768.

Bolshakov VY, Siegelbaum SA (1994) Postsynaptic induction and presynaptic expression of hippocampal long-term depression. Science 264:1148–1152.

Bristow J, Tee MK, Gitelman SE, Mellon SH, Miller WL (1993) Tenascin-X: a novel extracellular matrix protein encoded by the human XB gene overlapping P450c21B. J Cell Biol 122:265–278.

Bukalo O, Schachner M, Dityatev A (2001) Modification of extracellular matrix by enzymatic removal of chondroitin sulfate and by lack of tenascin-R differentially affects several forms of synaptic plasticity in the hippocampus. Neuroscience 104:359–369.

Cain DP (1997) LTP, NMDA, genes and learning. Curr Opin Neurobiol 7:235–242.

Cavus I, Koo PH, Teyler TJ (1996) Inhibition of long-term potentiation development in rat hippocampal slice by alpha 2-macroglobulin, an acute-phase protein in the brain. J Neurosci Res 43:282–288.

Chen G, Chen KS, Knox J, Inglis J, Bernard A, Martin SJ, Justice A, McConlogue L, Games D, Freedman SB, Morris RG (2000) A learning deficit related to age and beta-amyloid plaques in a mouse model of Alzheimer's disease. Nature 408:975–979.

Chiquet-Ehrismann R, Hagios C, Matsumoto K (1994) The tenascin gene family. Perspect Dev Neurobiol 2:3–7.

Christie BR, Schexnayder LK, Johnston D (1997) Contribution of voltage-gated Ca2+ channels to homosynaptic long-term depression in the CA1 region in vitro. J Neurophysiol 77:1651–1655.

Davis T, Buchberger JR, Malhotra JD, Xiao ZC, Schachner M, Braun PE, Isom LL (2001) Association between α and β1 subunits of neuronal sodium channels and tenascin-R. Soc Neurosci Abstr 27:46.8.

Eckhardt M, Bukalo O, Chazal G, Wang L, Goridis C, Schachner M, Gerardy-Schahn R, Cremer H, Dityatev A (2000) Mice deficient in the polysialyltransferase ST8SiaIV/PST-1 allow discrimination of the roles of neural cell adhesion molecule protein and polysialic acid in neural development and synaptic plasticity. J Neurosci 20:5234–5244.

Erickson HP (1994) Evolution of the tenascin family–implications for function of the C-terminal fibrinogen-like domain. Perspect Dev Neurobiol 2:9–19.

Faissner A, Schachner M (1995) Tenascin and janusin: Glial recognition molecules involved in neural development and regeneration. In: Neuroglia (Kettenmann H, Ransom BR, eds), pp 422–426. New York: Oxford University Press.

Ferhat L, Chevassus au LN, Jorquera I, Niquet J, Khrestchatisky M, Ben Ari Y, Represa A (1996) Transient increase of tenascin-C in immature hippocampus: astroglial and neuronal expression. J Neurocytol 25:53–66.

Forsberg E, Hirsch E, Frohlich L, Meyer M, Ekblom P, Aszodi A, Werner S, Fassler R (1996) Skin wounds and severed nerves heal normally in mice lacking tenascin-C. Proc Natl Acad Sci USA 93:6594–6599.

Fukamauchi F, Mataga N, Wang YJ, Sato S, Youshiki A, Kusakabe M (1996) Abnormal behavior and neurotransmissions of tenascin gene knockout mouse. Biochem Biophys Res Commun 221:151–156.

Gu H, Marth JD, Orban PC, Mossmann H, Rajewsky K (1994) Deletion of a DNA polymerase beta gene segment in T cells using cell type-specific gene targeting. Science 265:103–106.

Hagios C, Koch M, Spring J, Chiquet M, Chiquet-Ehrismann R (1996) Tenascin-Y: a protein of novel domain structure is secreted by differentiated fibroblasts of muscle connective tissue. J Cell Biol 134:1499–1512.

Hanse E, Gustafsson B (1992) Postsynaptic, but not presynaptic, activity controls the early time course of long-term potentiation in the dentate gyrus. J Neurosci 12:3226–3240.

Hoess RH, Ziese M, Sternberg N (1982) P1 site-specific recombination: nucleotide sequence of the recombining sites. Proc Natl Acad Sci USA 79:3398–3402.

Huang YY, Malenka RC (1993) Examination of TEA-induced synaptic enhancement in area CA1 of the hippocampus: the role of voltage-dependent Ca2+ channels in the induction of LTP. J Neurosci 13:568–576.

Huber KM, Mauk MD, Kelly PT (1995) Distinct LTP induction mechanisms: contribution of NMDA receptors and voltage-dependent calcium channels. J Neurophysiol 73:270–279.

Husmann K, Faissner A, Schachner M (1992) Tenascin promotes cerebellar granule cell migration and neurite outgrowth by different domains in the fibronectin type III repeats. J Cell Biol 116:1475–1486.

Jones PL, Jones FS (2000) Tenascin-C in development and disease: gene regulation and cell function. Matrix Biol 19:581–596.

Kang H, Welcher AA, Shelton D, Schuman EM (1997) Neurotrophins and time: different roles for TrkB signaling in hippocampal long-term potentiation. Neuron 19:653–664.

Kapur A, Yeckel MF, Gray R, Johnston D (1998) L-Type calcium channels are required for one form of hippocampal mossy fiber LTP. J Neurophysiol 79:2181–2190.

Kesner RP, Rolls ET (2001) Role of long-term synaptic modification in short-term memory. Hippocampus 11:240–250.

Kiernan BW, Gotz B, Faissner A, ffrench-Constant C (1996) Tenascin-C inhibits oligodendrocyte precursor cell migration by both adhesion-dependent and adhesion-independent mechanisms. Mol Cell Neurosci 7:322–335.

Kiernan BW, Garcion E, Ferguson J, Frost EE, Torres EM, Dunnett SB, Saga Y, Aizawa S, Faissner A, Kaur R, Franklin RJ, ffrench-Constant C (1999) Myelination and behaviour of tenascin-C null transgenic mice. Eur J Neurosci 11:3082–3092.

Lauri SE, Rauvala H, Kaila K, Taira T (1998) Effect of heparin-binding growth-associated molecule (HB-GAM) on synaptic transmission and early LTP in rat hippocampal slices. Eur J Neurosci 10:188–194.

Lipp HP, Wolfer DP (1998) Genetically modified mice and cognition. Curr Opin Neurobiol 8:272–280.

Maccaferri G, Toth K, McBain CJ (1998) Target-specific expression of presynaptic mossy fiber plasticity. Science 279:1368–1370.

Mackie EJ, Tucker RP (1999) The tenascin-C knockout revisited. J Cell Sci 112(Pt 22):3847–3853.

Maurice T, Su TP, Parish DW, Privat A (1995) Prevention of nimodipine-induced impairment of learning by the selective sigma ligand PRE-084. J Neural Transm Gen Sect 102:1–18.

McMonagle-Strucko K, Fanelli RJ (1993) Enhanced acquisition of reversal training in a spatial learning task in rats treated with chronic nimodipine. Pharmacol Biochem Behav 44:827–835.

Mellor J, Nicoll RA (2001) Hippocampal mossy fiber LTP is independent of postsynaptic calcium. Nat Neurosci 4:125–126.

Milev P, Fischer D, Haring M, Schulthess T, Margolis RK, Chiquet-Ehrismann R, Margolis RU (1997) The fibrinogen-like globe of tenascin-C mediates its interactions with neurocan and phosphacan/protein-tyrosine phosphatase-zeta/beta. J Biol Chem 272:15501–15509.

Miller S, Mayford M (1999) Cellular and molecular mechanisms of memory: the LTP connection. Curr Opin Genet Dev 9:333–337.

Mitrovic N, Schachner M (1995) Detection of tenascin-C in the nervous system of the tenascin-C mutant mouse. J Neurosci Res 42:710–717.

Morgan SL, Teyler TJ (2001) Electrical stimuli patterned after the theta-rhythm induce multiple forms of LTP. J Neurophysiol 86:1289–1296.

Morganti MC, Taylor J, Pesheva P, Schachner M (1990) Oligodendrocyte-derived J1–160/180 extracellular matrix glycoproteins are adhesive or repulsive depending on the partner cell type and time of interaction. Exp Neurol 109:98–110.

Morris RG, Garrud P, Rawlins JN, O'Keefe J (1982) Place navigation impaired in rats with hippocampal lesions. Nature 297:681–683.

Nagy A, Rossant J, Nagy R, Abramow-Newerly W, Roder JC (1993) Derivation of completely cell culture-derived mice from early-passage embryonic stem cells. Proc Natl Acad Sci USA 90:8424–8428.

Nakic M, Mitrovic N, Sperk G, Schachner M (1996) Kainic acid activates

transient expression of tenascin-C in the adult rat hippocampus. J Neurosci Res 44:355–362.
Nakic M, Manahan-Vaughan D, Reymann KG, Schachner M (1998) Long-term potentiation in vivo increases rat hippocampal tenascin-C expression. J Neurobiol 37:393–404.
Quartermain D, deSoria VG, Kwan A (2001) Calcium channel antagonists enhance retention of passive avoidance and maze learning in mice. Neurobiol Learn Mem 75:77–90.
Quevedo J, Vianna M, Daroit D, Born AG, Kuyven CR, Roesler R, Quillfeldt JA (1998) L-type voltage-dependent calcium channel blocker nifedipine enhances memory retention when infused into the hippocampus. Neurobiol Learn Mem 69:320–325.
Ratcliffe CF, Qu Y, McCormick KA, Tibbs VC, Dixon JE, Scheuer T, Catterall WA (2000) A sodium channel signaling complex: modulation by associated receptor protein tyrosine phosphatase beta. Nat Neurosci 3:437–444.
Riekkinen M, Schmidt B, Kuitunen J, Riekkinen P Jr (1997) Effects of combined chronic nimodipine and acute metrifonate treatment on spatial and avoidance behavior. Eur J Pharmacol 322:1–9.
Saga Y, Yagi T, Ikawa Y, Sakakura T, Aizawa S (1992) Mice develop normally without tenascin. Genes Dev 6:1821–1831.
Saghatelyan AK, Gorissen S, Albert M, Hertlein B, Schachner M, Dityatev A (2000) The extracellular matrix molecule tenascin-R and its HNK-1 carbohydrate modulate perisomatic inhibition and long-term potentiation in the CA1 region of the hippocampus. Eur J Neurosci 12:3331–3342.
Saghatelyan AK, Dityatev A, Schmidt S, Schuster T, Bartsch U, Schachner M (2001) Reduced perisomatic inhibition, increased excitatory transmission, and impaired long-term potentiation in mice deficient for the extracellular matrix glycoprotein tenascin-R. Mol Cell Neurosci 17:226–240.
Sambrook J, Fritsch EF, Maniatis T (1989) Molecular cloning: a laboratory manual.
Sandin M, Jasmin S, Levere TE (1990) Aging and cognition: facilitation of recent memory in aged nonhuman primates by nimodipine. Neurobiol Aging 11:573–575.
Saucier D, Cain DP (1995) Spatial learning without NMDA receptor-dependent long-term potentiation. Nature 378:186–189.
Settles DL, Kusakabe M, Steindler DA, Fillmore H, Erickson HP (1997) Tenascin-C knockout mouse has no detectable tenascin-C protein. J Neurosci Res 47:109–117.
Shapiro ML, Eichenbaum H (1999) Hippocampus as a memory map: synaptic plasticity and memory encoding by hippocampal neurons. Hippocampus 9:365–384.
Shimizu E, Tang YP, Rampon C, Tsien JZ (2000) NMDA receptor-dependent synaptic reinforcement as a crucial process for memory consolidation. Science 290:1170–1174.
Shors TJ, Matzel LD (1997) Long-term potentiation: what's learning got to do with it? Behav Brain Sci 20:597–614.
Snow DM, Atkinson PB, Hassinger TD, Letourneau PC, Kater SB (1994) Chondroitin sulfate proteoglycan elevates cytoplasmic calcium in DRG neurons. Dev Biol 166:87–100.
Song D, Xie X, Wang Z, Berger TW (2001) Differential effect of TEA on long-term synaptic modification in hippocampal CA1 and dentate gyrus in vitro. Neurobiol Learn Mem 76:375–387.
Srinivasan J, Schachner M, Catterall WA (1998) Interaction of voltage-gated sodium channels with the extracellular matrix molecules tenascin-C and tenascin-R. Proc Natl Acad Sci USA 95:15753–15757.
Steindler DA, Settles D, Erickson HP, Laywell ED, Yoshiki A, Faissner A, Kusakabe M (1995) Tenascin knockout mice: barrels, boundary molecules, and glial scars. J Neurosci 15:1971–1983.
Strekalova T, Sun M, Sibbe M, Evers M, Dityatev A, Gass P, Schachner M (2002) Fibronectin domains of extracellular matrix molecule tenascin-C modulate hippocampal learning and synaptic plasticity. Mol Cell Neurosci (in press).
Thibault O, Landfield PW (1996) Increase in single L-type calcium channels in hippocampal neurons during aging. Science 272:1017–1020.
Thibault O, Hadley R, Landfield PW (2001) Elevated postsynaptic [Ca2+]i and L-type calcium channel activity in aged hippocampal neurons: relationship to impaired synaptic plasticity. J Neurosci 21:9744–9756.
Towbin H, Staehelin T, Gordon J (1979) Electrophoretic transfer of proteins from polyacrylamide gels to nitrocellulose sheets: procedure and some applications. Proc Natl Acad Sci USA 76:4350–4354.
Tsien JZ, Huerta PT, Tonegawa S (1996) The essential role of hippocampal CA1 NMDA receptor-dependent synaptic plasticity in spatial memory. Cell 87:1327–1338.
Weber P, Montag D, Schachner M, Bernhardt RR (1998) Zebrafish tenascin-W, a new member of the tenascin family. J Neurobiol 35:1–16.
Weber P, Bartsch U, Rasband MN, Czaniera R, Lang Y, Bluethmann H, Margolis RU, Levinson SR, Shrager P, Montag D, Schachner M (1999) Mice deficient for tenascin-R display alterations of the extracellular matrix and decreased axonal conduction velocities in the CNS. J Neurosci 19:4245–4262.
Weisskopf MG, Castillo PE, Zalutsky RA, Nicoll RA (1994) Mediation of hippocampal mossy fiber long-term potentiation by cyclic AMP. Science 265:1878–1882.
Wood ER, Dudchenko PA, Robitsek RJ, Eichenbaum H (2000) Hippocampal neurons encode information about different types of memory episodes occurring in the same location. Neuron 27:623–633.
Zamanillo D, Sprengel R, Hvalby O, Jensen V, Burnashev N, Rozov A, Kaiser KM, Koster HJ, Borchardt T, Worley P, Lubke J, Frotscher M, Kelly PH, Sommer B, Andersen P, Seeburg PH, Sakmann B (1999) Importance of AMPA receptors for hippocampal synaptic plasticity but not for spatial learning. Science 284:1805–1811.
Zeng H, Chattarji S, Barbarosie M, Rondi-Reig L, Philpot BD, Miyakawa T, Bear MF, Tonegawa S (2001) Forebrain-specific calcineurin knockout selectively impairs bidirectional synaptic plasticity and working/episodic-like memory. Cell 107:617–629.
Zhou XH, Brakebusch C, Matthies H, Oohashi T, Hirsch E, Moser M, Krug M, Seidenbecher CI, Boeckers TM, Rauch U, Buettner R, Gundelfinger ED, Fassler R (2001) Neurocan is dispensable for brain development. Mol Cell Biol 21:5970–5978.